Quaternary Science Reviews 182 (2018) 93–108

Contents lists available at ScienceDirect

Quaternary Science Reviews

journal homepage: www.elsevier.com/locate/quascirev

Changes in sea ice cover and ice sheet extent at the Yermak Plateau during the last 160 ka – Reconstructions from biomarker records

A. Kremer [a, *], R. Stein [a], K. Fahl [a], Z. Ji [b], Z. Yang [b], S. Wiers [c], J. Matthiessen [a], M. Forwick [d], L. Löwemark [e], M. O'Regan [e], J. Chen [b], I. Snowball [c]

[a] Alfred Wegener Institute, Helmholtz Centre for Polar and Marine Research, Germany
[b] Key Laboratory of Marine Ecosystem and Biogeochemistry, Second Institute of Oceanography, State Oceanic Administration, Hangzhou, China
[c] Uppsala University, Sweden
[d] UiT The Arctic University of Norway, Norway
[e] Stockholm University, Sweden

ARTICLE INFO

Article history:
Received 17 November 2017
Accepted 18 December 2017
Available online 9 January 2018

ABSTRACT

The Yermak Plateau is located north of Svalbard at the entrance to the Arctic Ocean, i.e. in an area highly sensitive to climate change. A multi proxy approach was carried out on Core PS92/039-2 to study glacial-interglacial environmental changes at the northern Barents Sea margin during the last 160 ka. The main emphasis was on the reconstruction of sea ice cover, based on the sea ice proxy IP_{25} and the related phytoplankton - sea ice index PIP_{25}. Sea ice was present most of the time but showed significant temporal variability decisively affected by movements of the Svalbard Barents Sea Ice Sheet. For the first time, we prove the occurrence of seasonal sea ice at the eastern Yermak Plateau during glacial intervals, probably steered by a major northward advance of the ice sheet and the formation of a coastal polynya in front of it. Maximum accumulation of terrigenous organic carbon, IP_{25} and the phytoplankton biomarkers (brassicasterol, dinosterol, HBI III) can be correlated to distinct deglaciation events. More severe, but variable sea ice cover prevailed at the Yermak Plateau during interglacials. The general proximity to the sea ice margin is further indicated by biomarker (GDGT) - based sea surface temperatures below 2.5 °C.

© 2017 Elsevier Ltd. All rights reserved.

1. Introduction

The decline of Arctic sea ice began to draw attention in 2005, when summer sea ice reached the lowest extent since satellite based observations started in 1979 (Serreze et al., 2007). Having enlivened the debate around anthropogenic climate change, this dramatic trend continued - much faster than forecast - when a new record low in sea ice extent was reached in 2007 followed by another in 2012 (Comiso et al., 2008; Parkinson and Comiso, 2013). Most recently, the maximum winter extent of Arctic sea ice reached a record minimum in 2016 (National Snow & Ice Data Center, https://nsidc.org). Playing a crucial role in maintaining climatic stability worldwide, such a development of Arctic sea ice is alarming, even more when polar amplification of global warming is taken into account (Serreze and Barry, 2011). Arctic sea ice impacts the Earth's global energy budget through regulating the surface albedo, controls the exchange of heat and moisture between the atmosphere and the ocean, contributes to global heat transfer and influences local primary production (Broecker, 1997; Hall, 2004; Dieckmann and Hellmer, 2008). Despite this fundamental relevance of Arctic sea ice, our understanding of its interaction with different internal and external forces is still incomplete for certain regions and timespans. In order to improve climate predictions and related measures, it is essential to know how this sensitive system responds to climatic variations. To evaluate the anthropogenic impact on sea ice decline, it is imperative to extend records of past sea ice extent beyond the modern observational period.

The Yermak Plateau north of Svalbard is located at the interface between the Arctic Ocean and the Atlantic Ocean. This area is subject to a range of environmental forces, e.g., the intensity of various ocean currents and the glaciation on Svalbard. Throughout the late Quaternary, the Svalbard Barents Sea Ice Sheet (SBIS) advanced several times towards the shelf break along western and northern Svalbard, strongly impacting oceanic conditions and

* Corresponding author.
E-mail address: akremer@awi.de (A. Kremer).

https://doi.org/10.1016/j.quascirev.2017.12.016
0277-3791/© 2017 Elsevier Ltd. All rights reserved.

sedimentation regimes (e.g., Svendsen et al., 2004; Winkelmann et al., 2008a; Knies et al., 2009; Jessen et al., 2010). According to the glaciation model of Mangerud et al. (1998), four major ice sheets built up and decayed along western Svalbard during the last 150 ka: the most extensive one during the late Saalian (>140 ka), followed by an early (~110 ka), a middle (60 ka) and a late Weichselian glaciation (~20 ka; Landvik et al., 1998; Mangerud et al., 1998; Hughes et al., 2016). The northernmost extent as well as local discrepancies are, however, still under debate and need further investigation (Winkelmann et al., 2008a; Clark et al., 2009; Ingólfsson and Landvik, 2013; Landvik et al., 2013). Intensified Atlantic Water (AW) advection via the West Spitsbergen Current (WSC) and related open water areas in the Greenland, Iceland and Norwegian Seas are believed to be an important trigger for ice sheet growth by providing extensive amounts of moisture (Hebbeln et al., 1994; Dokken and Hald, 1996). The strongest inflow of warm AW was recorded for the Eemian and the Holocene (Henrich, 1998; Knies et al., 1999; Matthiessen et al., 2001; Matthiessen and Knies, 2001; Wollenburg et al., 2001; Spielhagen et al., 2004). Less pronounced advection was observed for MIS 5c, 5a and 3, while the glacial periods MIS 6, 4 and 2 were characterised by persistent but modified (temperate) inflow (Henrich, 1998; Knies et al., 1999).

The main objective of the current study is to reconstruct sea ice variability in the northernmost Fram Strait related to late Quaternary glacial-interglacial cycles. For this purpose, measurements of specific biomarkers were carried out on Core PS92/039-2 from the Yermak Plateau north of Svalbard. Supplemented by a set of organic and sedimentological parameters (lithology, IRD, TOC, C/N ratio), these biomarker data provide a solid base to outline the environmental development of the Fram Strait during the last 160 ka.

2. Biomarker proxies used for paleoenvironmental reconstruction in this study

The organic-geochemical investigation of marine archives with regard to specific molecular signatures (biomarkers) has been a common practice in paleoenvironmental studies for some time (e.g., Meyers, 1997; Stein and Macdonald, 2004; Volkman, 2006; Eglinton and Eglinton, 2008; Sachs et al., 2013). In this study, the main focus is on the reconstruction of past sea ice cover, with estimates of the sea surface temperature (SST) serving as additional verification. Furthermore, the production of marine, open-water phytoplankton (hereafter referred to as “phytoplankton”) and the input of terrigenous material are assessed using specific biomarkers.

In the past decade, the novel sea ice proxy IP_{25} (C_{25} HBI [highly branched isoprenoid] monoene = IP_{25}; Belt et al., 2007) paved the way for reconstructing the variability of past sea ice conditions in the Arctic realm, reaching back to the late Miocene (Stein et al., 2016). Biosynthesised by diatoms exclusively living in Arctic sea ice (Belt et al., 2008; Brown et al., 2014), the presence/absence of this organic molecule in sediment samples serves as a presence/absence indicator for spring sea ice cover (Belt et al., 2007). An even more reliable estimate of sea ice conditions is achieved when combining IP_{25} with phytoplankton biomarkers, creating the PIP_{25} index (phytoplankton marker − IP_{25} = PIP_{25}; Müller et al., 2011). In this way, the problem of misjudging absent IP_{25}, either reflecting perennial ice cover or ice-free water, can be circumvented.

Although the principle of this approach is convincing, existing limitations should be considered when using PIP_{25} for sea ice reconstructions. Difficulties may arise when in-phase fluxes of the phytoplankton marker and IP_{25} occur (Müller et al., 2011). In this case, coevally low (indicating permanent sea ice conditions) or high (indicating marginal sea ice conditions) input would result in similar PIP_{25} values and a misleading sea ice evaluation. Therefore, it is key to always consider the individual biomarker profiles alongside the PIP_{25} record. The sterols brassicasterol and dinosterol are commonly used as phytoplankton markers in the PIP_{25} (P_BIP_{25} and P_DIP_{25}, respectively) calculation. As these sterols are biosynthesised by a relatively broad group of marine phytoplankton, mainly diatoms and dinoflagellates (Boon et al., 1979; Robinson et al., 1984; Volkman et al., 1998), their sedimentary signal represents various environmental conditions. Further, the PIP_{25}-based sea ice reconstructions may be biased by selective biomarker degradation of the structurally differing IP_{25} and sterol compounds (for a detailed review of potential limitations of the PIP_{25} approach, see Stein et al., 2012; Navarro-Rodriguez et al., 2013; Belt and Müller, 2013).

Despite potential limitations, both P_BIP_{25} and P_DIP_{25} indices show a positive correlation with modern satellite-based sea ice observations (Müller et al., 2012; Xiao et al., 2015a) and have been used to define paleo sea ice conditions more quantitatively in a variety of studies (e.g., Müller et al., 2012; Stein and Fahl, 2013; Müller and Stein, 2014; Belt et al., 2015; Xiao et al., 2015b; Hörner et al., 2016; Stein et al., 2017a).

Nonetheless, the adoption of a more suitable open water counterpart to IP_{25} is recently investigated with special attention to a tri-unsaturated HBI lipid (HBI III, Belt et al., 2000, 2015; Smik et al., 2016). The HBI III compound is found in marine sediments of temperate regions worldwide but is especially enriched within the Marginal Ice Zone (MIZ; transition between open ocean and sea ice) of the Arctic Ocean (Belt et al., 2000, 2015). Even though the specific source of this compound is not identified unequivocally, the only known producers are marine diatoms (Belt et al., 2000; Rowland et al., 2001). The concentrations of IP_{25} and HBI III are much closer in magnitude than IP_{25} and brassicasterol or dinosterol, potentially superseding the need of the concentration balance factor currently used in the PIP_{25} quantification (Belt et al., 2015; Smik et al., 2016; see also “Material and methods”). The $P_{III}IP_{25}$ approach already enabled reliable paleo sea ice reconstructions by Belt et al. (2015), Berben et al. (2017) and Stein et al. (2017b). However, the applicability of this approach needs to be evaluated by further analysis of downcore records and the correlation of surface data sets to satellite-derived sea ice observations.

For temperature reconstruction, the alkenone - based U^k_{37} index (Brassell et al., 1986; Prahl and Wakeham, 1987) and the GDGT (glycerol dialkyl glycerol tetraether) - based TEX_{86} index (Schouten et al., 2002) are two common organic-geochemical tools in paleoceanographic studies. While correlating well with SSTs in tropical and temperate regions, these approaches show large inaccuracies in regions dominated by colder water masses (Kim et al., 2008). The modified TEX^L_{86} index for temperatures below 15 °C (Kim et al., 2010) yields a better correlation but still anomalously high temperatures for the Arctic Ocean (Ho et al., 2014). Liu et al. (2012) identified GDGTs with an additional hydroxyl group on the alkyl chain. These hydroxylated GDGTs (OH-GDGTs) likely originate from planktonic archaea and are widespread in marine surface and downcore sediments (Liu et al., 2012; Fietz et al., 2013). Both the relative abundance of individual OH-GDGTs and the number of their cyclopentane rings vary with temperature (Fietz et al., 2013), leading to the development of the ring index RI-OH (Lü et al., 2015). The revised RI-OH′ index includes specific OH-GDGTs more abundant in polar regions, therefore possibly representing a promising tool for the reconstruction of temperatures in this specific environment. This study will use the RI-OH’ index for the first time to calculate polar SSTs, thereby providing important information about its applicability in high latitudes.

For the source identification of organic matter in marine sediments, a variety of organic-geochemical bulk parameters (e.g., C/N

ratio, $\delta^{13}C_{org}$ values, Rock-Eval parameters) and specific biomarkers (e.g., *n*-alkanes, sterols) can be applied (Meyers, 1997; Stein and Macdonald, 2004). The signals given by these different proxies may vary, however, when used in combination, a solid evaluation of the relative proportions of marine and terrigenous organic matter can be attained (e.g., Fahl and Stein, 2007; Volkman et al., 2008). To infer contributions of terrigenous material, this study concentrated on the sterols β-sitosterol and campesterol (Pryce, 1971; Huang and Meinschein, 1979). Although these biomarkers are found in a few microalgae species, the main contributors are higher land plants (Volkman, 1986; Jaffé et al., 1995; Rontani et al., 2014) that are delivered to the Arctic Ocean through Siberian river runoff (Fahl et al., 2003; Fahl and Stein, 2007). In order to ensure the credibility of these results, further proxies (i.e., C/N ratio, $\delta^{13}C_{org}$ values) were applied to trace terrigenous input mechanisms.

3. Regional setting

The Yermak Plateau is located at the entrance to the Arctic Ocean off the north-western coast of Svalbard (Fig. 1). To the west of the plateau, the Fram Strait, representing the northernmost North Atlantic, displays the only deepwater connection between the Arctic Ocean and the world oceans. Two major ocean current systems regulate the exchange of water masses in this gateway, thereby generating an Atlantic and an Arctic domain: the WSC and the East Greenland Current (EGC), respectively (Aagaard and Coachman, 1968; Aagaard, 1982). Steered by bathymetry, the relatively warm WSC flows in intermediate depth northward along the western continental margin of Svalbard (Bourke et al., 1988). Between 78 and 80°N, the WSC bifurcates into an eastern (Svalbard) branch and a western (Yermak) branch (Aagaard et al., 1987; Manley et al., 1992). The Svalbard Branch streams northeasterly, staying close to the continental margin of Svalbard, and eventually enters the Arctic Ocean (Coachman and Aagaard, 1974; Aagaard et al., 1987; Manley, 1995). The Yermak Branch follows the western flank of the Yermak Plateau, partly detaches from it north of 80°N, turns westward and recirculates southward as the Return Atlantic Current (Bourke et al., 1988). Cold polar water and sea ice exit the Arctic Ocean along the continental margin of East Greenland via the southward streaming EGC (Aagaard and Coachman, 1968; Rudels et al., 1999). Positioned within the narrow MIZ, the study area is subject to a pronounced seasonality. The formation of new sea ice is mainly restricted to the autumn and winter months, while summer is the season of ice melt. When sea ice extent reaches its maximum in March, the Svalbard Archipelago is usually largely enclosed by ice. However, upwelling of relatively warm AW along the western and northern coast ensures ice free conditions up to 80–82°N (Aagaard et al., 1987; Haugan, 1999; Ivanov et al., 2012). The extension of these open water areas (polynyas) depends on the intensity of the WSC and shows a strong interannual variability (Vinje, 2001). Minimum sea ice cover is reached in September, only the northeastern shelf areas of Svalbard may experience sea ice during this time of the year. While the southern Yermak Plateau is covered by seasonal sea ice, a thinning of the perennial ice cover above the northern part only takes place in years of exceptionally strong heat supply (National Snow & Ice Data Center, https://nsidc.org).

4. Material and methods

The studied Core PS92/039-2 was recovered from the eastern flank of the Yermak Plateau north of Svalbard during RV Polarstern Expedition PS92 in 2015 (Peeken, 2016, Fig. 1; Table 1). It provides a continuous sedimentary record, except for the uppermost 15 cm that were disturbed during the recovery process (Supplementary Fig. 1). Therefore, a surface sample from the box-corer Core PS92/039-3 (Table 1) was added to the record to have a reference data point representing the modern (Holocene) environment. Line-scan images (performed at the UiT the Arctic University of Norway in Tromsø) were acquired with a Jai CV L107 camera with RGB (red-green-blue) channels at 630 nm, 535 nm and 450 nm, respectively, mounted to an Avaatech XRF core scanner. For environmental magnetic measurements, samples were taken continuously (2.5–3 cm interval) with standard 7 cm^3 plastic cubes. Low field reversible magnetic susceptibility (k) was measured with an Agico MFK-1-FA Kappabridge (performed at Uppsala University, Sweden). Anhysteretic remanent magnetisation (ARM) was acquired in a peak alternating field of 100 mT with a 50 μT DC bias field and measured using cryogenic magnetometer (model 2G Enterprise 755R, performed at the University of Bremen, Germany). The

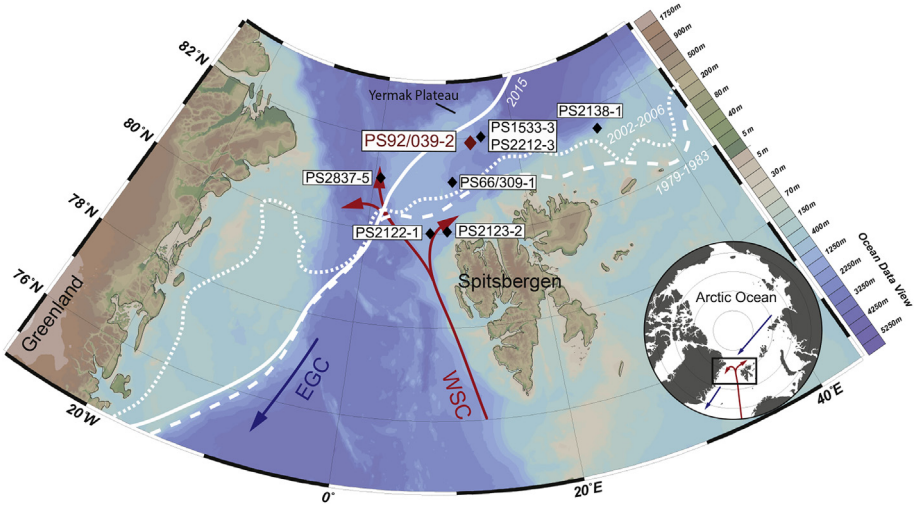

Fig. 1. Overview map of the Arctic Ocean (inset) and the oceanographic setting in the study area. The red arrow refers to the West Spitsbergen Current (WSC), the blue arrow indicates the East Greenland Current (EGC). The position of the September sea ice margin for the time intervals 1979–1983 and 2002–2006 is marked by white, dotted lines, the sea ice extent during September 2015 is indicated by a white, solid line (http://iup.physik.uni-bremen.de). Core locations are marked by diamonds, the herein investigated Core PS92/039-2 is highlighted in red. (For interpretation of the references to colour in this figure legend, the reader is referred to the Web version of this article.)

susceptibility of ARM (kARM) was calculated from ARM measurements normalised with the 50 μT bias field. Subsequent division with the magnetic susceptibility yields the dimensionless magnetic grain-size sensitive ratio kARM/k (King et al., 1982).

4.1. Analyses of organic-geochemical bulk parameters

For organic-geochemical analyses, subsamples were taken every 5 cm and stored in glass vials at −20 °C. Total organic carbon (TOC) contents were determined using a Carbon-Sulfur Analyser (CS-125, Leco) after decarbonisation of the sediment with hydrochloric acid. The total amounts of carbon (TC) and nitrogen (TN) were determined by means of a Carbon-Nitrogen-Sulfur Analyser (Elementar III, Vario). Assuming that the predominant carbonate phase is calcite, carbonate contents were calculated as $CaCO_3 = (TC - TOC) * 8.333$, where 8.333 is the stoichiometric calculation factor. When using the carbonate data, however, one should consider that a significant proportion of the carbonate at the Yermak Plateau might be dolomite as determined in sediments from nearby Core PS2212-3 (Fig. 1; Vogt, 1997; Vogt et al., 2001). The C/N ratio was calculated using the TOC and TN contents, thereby neglecting the inorganic nitrogen portion (cf., Stein and Macdonald, 2004; Supplementary Fig. 2). For organic carbon isotope ($\delta^{13}C_{org}$) analysis (performed at the Second Institute of Oceanography, State Oceanic Administration, Hangzhou, China), acidified and homogenised sediment was weighed into a tin foil and wrapped tightly. The determination of $\delta^{13}C_{org}$ values was then performed by means of mass spectrometry (Thermo, MAT 253), using Urea Isotopic Working Standard (C-13, N-15) as reference material.

4.2. Biomarker analyses

For HBIs and sterol analyses, 5 g of freeze-dried and ground sediment was extracted with an Accelerated Solvent Extractor (DIONEX, ASE 200; 100 °C, 5 min, 1000 psi) using dichloromethane:methanol (2:1 vol/vol) as solvent. Beforehand, the internal standards 7-hexylnonadecane (7-HND; 0.076 μg/sample) and cholesterol-d6 (cholest-5-en-3β-ol-D_6; 10.1 μg/sample) were added for biomarker quantification. Hydrocarbons and sterols were separated via open column chromatography using SiO_2 as stationary phase and 5 ml of *n*-hexane followed by 6 ml of ethylacetate:*n*-hexane (2:8 vol/vol) as eluent, respectively. Sterols were silylated with 200 μl bis-trimethylsilyl-trifluoroacet-amide (BSTFA; 60 °C, 2 h) in the next step. Compound identification was carried out with coupled gas chromatography (GC) – mass spectrometry (MS; Agilent 7890B GC - Agilent 5977 A for HBI identification, Agilent 6850 GC - Agilent 5975 C for sterol identification). GC measurements were carried out with the following temperature setup: 60 °C (3 min), 150 °C (heating rate: 15 °C/min), 320 °C (heating rate: 10 °C/min), 320 °C (15 min isothermal) for the hydrocarbons and 60 °C (2 min), 150 °C (heating rate: 15 °C/min), 320 °C (heating rate: 3 °C/min), 320 °C (20 min isothermal) for the sterols. Helium served as carrier gas (1 ml/min constant flow). Specific compound identification was based on the comparison of retention times and mass spectra with literature references (sterols: Boon et al., 1979; Volkman, 1986; HBIs: Belt et al., 2007; Brown and Belt, 2016). The concentration of each biomarker was calculated by setting its individual GC-MS ion responses in relation to those of respective internal standards. For the quantification of the sterols (quantified as trimethylsilyl ethers), the molecular ions m/z 470 for brassicasterol (as 24-methylcholesta-5,22E-dien-3β-ol), m/z 472 for campesterol (as 24-methylcholest-5-en-3β-ol), m/z 486 for β-sitosterol (as 24-ethylcholest-5-en-3β-ol) and m/z 500 for dinosterol (as 4α,23,24R-trimethyl-5α-cholest-22E-en-3β-ol) were used in relation to the molecular ion m/z 464 for the internal standard cholesterol-d_6. For the quantification of IP_{25} and HBI III, their molecular ions (m/z 350 for IP_{25} and m/z 346 for HBI III) were compared to the molecular ion m/z 266 for the internal standard 7-HND. The different responses of these ions were balanced by an external calibration curve (see Fahl and Stein, 2012). All biomarker concentrations were normalised to the amount of extracted sediment and organic carbon (OC) content.

To avoid over- or underestimating the sea ice signal, PIP_{25} indices were calculated following the equation of Müller et al. (2011): $P_BIP_{25} = IP_{25}/(IP_{25}+(\text{brassicasterol}*c))$, where c is a balance factor to compensate significant concentration differences between IP_{25} and brassicasterol (c = mean IP_{25} concentration/mean brassicasterol concentrations). Additionally, $P_{III}IP_{25}$ indices were calculated using HBI III as phytoplankton marker.

For GDGT analyses (performed at the Second Institute of Oceanography, State Oceanic Administration, Hangzhou, China), 5–10 g of sediment (freeze-dried, ground) was ultrasonically extracted using dichloromethane:methanol (3:1 vol/vol) as solvent. Prior to this step, the internal standard C46 (0.378 μg/sample) was added to the sample. The alcohol fraction containing GDGTs was eluted via open column chromatography using silica gel as stationary phase and dichloromethane:methanol (10 ml; 95:5 vol/vol) as solvent. Compound identification was performed with ultra performance liquid chromatography (Acquity) coupled to atmospheric pressure chemical ionisation mass spectrometry (Xevo TQ MS). The GDGTs were eluted using E1(hexane):E2(hexane:isopropanol) (99:1 vol/vol), with 0.1% isopropanol for 0.5 min (flow rate: 0.2 ml/min), then with linear gradient up to 0.5% in 0.6 min (3.5 min isothermal), followed by up to 1% in 1.4 min (2 min isothermal) and finally to 0.1% (4 min isothermal). Single ion recording was set to scan $[M+H]^+$ of isoprenoid glycerol dibiphytanyl glycerol tetraethers (OH-GDGT-0, OH-GDGT-1, OH-GDGT-2, i-GDGT-0, i-GDGT-1, i-GDGT-2, i-GDGT-3, Crenarchaeol, Cren'; m/z 1318, 1316,1314, 1302, 1300, 1298, 1296, 1292, 1292, respectively) and $[M+H]^+$ of the branched-GDGTs (b-GDGT Ia, b-GDGT IIa, b-GDGT IIIa; m/z 1050, 1036, 1022, respectively). SSTs were calculated using the ring index of OH-GDGTs (Supplementary Fig. 3), recommended for polar regions, following the equations presented by Lü et al. (2015): RI-OH' = ([OH-GDGT-1] + 2*[OH-GDGT-2])/([OH-GDGT-0] + [OH-GDGT-1] + [OH-GDGT-2]) and RI-OH' = 0.0382 * SST + 0.1. All data are available online on PANGAEA.

5. Results

5.1. Lithology and ice rafted debris (IRD)

In the lowermost part of the core (860 - 615 cm), the dominant lithotypes are silty clays intercalated by diamicton layers. An alternation of greyish, dark greyish and brownish coloured

Table 1
Investigated cores.

Core-ID	Latitude [°N]	Longitude [°E]	Water depth [m]	Core recovery [cm]
PS92/039-2 KAL	81.95	13.83	1464	860
PS92/039-3 GKG	81.94	13.75	1493	43

intervals can be observed. The overlaying sequence from 615 to 90 cm consists of clayey to silty clayey sediments with a greyish to brownish colour spectrum. Two layers of dark greyish colouration are conspicuous between 310 - 260 cm and 140 - 90 cm. The upper 90 cm are composed of brownish sediments (Supplementary Fig. 1). Various bioturbation traces are present throughout the entire record, except for short intervals around 730, 580, 510, 365 and 275 cm (Supplementary Fig. 1). Peak abundance of IRD (counted on x-radiographs) can be observed in the intervals 650–600, 250–200 and 145–120 cm, while lower amounts of IRD grains are found in 590–310 cm core depth (Fig. 2).

5.2. Organic-geochemical bulk parameters

The TOC content ranges from 0.2 to 1.3% with slightly enhanced values from 860 to 610 cm as well as distinct maxima from 310 to 250 cm and 140 to 90 cm (Fig. 2). The C/N ratio varies between 4 and 18 in the lowermost part of the core, then changes to slightly lower (~7) and more stable values above 610 cm and lowest values at the surface (~2). Similar to the TOC record, elevated values in the C/N ratio can be observed for the intervals from 310 to 250 cm (up to 12) and 140–90 cm (up to 10). The carbonate record shows a highly fluctuating signal around an average of 4% (Fig. 2). At 415 cm, a sharp rise to a maximum content of 12% occurs, followed by a sudden drop to mean values at 350 cm core depth. From 70 cm upwards, another sharp increase in the carbonate content occurs with peak values of 13% at the surface.

The $\delta^{13}C_{org}$ record is relatively balanced with values ranging between ~ -23 to ~ -25‰, except for short-term shifts to lighter values (−27‰) at 180 and 640 cm.

5.3. Biomarkers

The biomarker concentrations vary synchronously and in phase throughout the entire record (Fig. 2). For the lowermost part of the core, highly fluctuating concentrations can be observed with maximum contents of 0.0030 μg/g sediment for IP_{25}, 0.0120 μg/g sediment for HBI III, 0.61 μg/g sediment for brassicasterol, 0.15 μg/g sediment for dinosterol and 0.72 μg/g sediment for the terrigenous sterols. At 680 cm core depth, biomarker contents decrease and remain at minimum concentrations to a depth of 390 cm. IP_{25} is mostly absent within this sequence. However, short-term excursions to elevated concentrations occur at 640, 530 and 450 cm (up to 0.0014, 0.0025, 0.25, 0.09 and 0.29 μg/g sediment for IP_{25}, HBI III, brassicasterol, dinosterol and the terrigenous sterols, respectively). The sediment sequence between 390 and 90 cm shows a succession of intervals with either minimal to absent and relatively high to maximum biomarker contents (IP_{25}, HBI III, brassicasterol, dinosterol and the terrigenous sterols reach maximum values of 0.0051, 0.0451, 0.72, 0.16 and 1.77 μg/g sediment, respectively). Most prominent peaks occur between 310 - 250 and 150 - 90 cm core depth. These peaks coincide with the most conspicuous excursions to higher values in the TOC and C/N records (Fig. 2). At 90 cm, a drop of all biomarkers to minor concentrations is observed that continues to the uppermost core interval. Between 90 and 40 cm, IP_{25} is completely absent. The surface sample shows enhanced biomarker contents of 0.0071 μg/g sediment for HBI III for IP_{25}, 0.0050 μg/g sediment for HBI III, 1.32 μg/g sediment for brassicasterol, 0.07 μg/g sediment for dinosterol and 0.46 μg/g sediment for the terrigenous sterols (Fig. 2). The absolute biomarker concentrations in the surface sample are several orders of magnitude higher than the downcore concentrations. This strong gradient refers to the early biogeochemical degradation of biomarkers in the water column and the upper centimetre of the sediment (Fahl and Stein, 2012; Belt and Müller, 2013).

6. Discussion

6.1. Age model

The chronostratigraphy of Core PS92/039-2 is based on a combination of AMS^{14}C dates (Table 2) as well as tie points obtained from core correlation and biostratigraphy (Table 3).

In the upper part of the core, a significant decrease in the carbonate content and a minimum followed by a maximum in the magnetic susceptibility log are correlated to corresponding trends at Core PS1533-3 (Figs. 1 and 3). This core is located in close vicinity to Core PS92/039-2 and has a well-established age model based on radiocarbon dates and $\delta^{18}O$ stratigraphy for the last 30 ka (Spielhagen et al., 2004). The correlation is further substantiated by similar deflections of the carbonate and magnetic susceptibility records observed in the nearby cores PS2212-3 (Vogt, 1997) and PS66/309-1 (Winkelmann et al., 2008a,b). Further downcore, three AMS^{14}C ages at 150, 227.5 and 298 cm allow to pinpoint MIS 2 and 3 in Core PS92/039-2 (Table 2). The distinct minima in magnetic susceptibility and magnetic grain size sensitive kARM/k ratio in Core PS92/039-2 at 320 to 260 cmbsf, based on AMS^{14}C dating slightly younger than 44.8 ka, can be correlated well to corresponding values of Core PS1533-3 (Fig. 3). Originally, these minima in Core PS1533-3 were dated to MIS 4 (Spielhagen et al., 2004), but our new data suggest a MIS 3 age. Further investigation is needed to clarify these discrepancies, this study, however, relies on the AMS^{14}C ages. The occurrence of the biostratigraphic marker *Pullenia bulloides* at 388 cm (Peeken, 2016) is considered to indicate MIS event 5.1 (~81 ka, Haake and Pflaumann, 1989), as in the cores PS2212-3, PS2122 and PS2123 (Vogt, 1997; Vogt et al., 2001). The MIS 5/6 boundary is well-defined in nearby Core PS1533-3, based on ^{10}Be- and $\delta^{18}O$-stratigraphy (Nowaczyk et al., 1994; Spielhagen et al., 2004). A decrease of the magnetic susceptibility at this transition is also recorded for the cores PS2212-3 (Nowaczyk et al., 1994) and PS66/309-1 (Winkelmann et al., 2008b) and for Core PS92/039-2, ensuring a clear allocation of this stage boundary to 610 cm core depth. According to linear extrapolation, the core base is of early MIS 6 age (~180 ka; Fig. 4). This estimation is, however, unrealistic given the fact that the sedimentation rates of MIS 6 most likely differ from those of MIS 5. Previous studies north of Spitsbergen described significantly higher sedimentation rates in MIS 6 compared to the following MIS 5 interval (Knies et al., 2001; Stein et al., 2001; Winkelmann et al., 2008a). In the neighbouring Core PS66/309-1, the sedimentation rates of MIS 6 exceed those of MIS 5 by a factor of ~2 (Winkelmann et al., 2008a). Assuming similar changes for Core PS92/039-2, the more probable age of the core base is ~160 ka (Fig. 4).

An additional, independent confirmation of this age model is given by the mineral magnetic data, i.e., the kARM/k ratio representing a magnetic mineral grain size proxy. Previous studies have described a noticeable similarity between the kARM/k ratio and $\delta^{18}O$ data (Nowaczyk et al., 1994; O'Regan et al., 2008; Xuan et al., 2012). Thus, the correlation of this ratio at Core PS92/039-2 to the global benthic $\delta^{18}O$ record of Lisiecki and Raymo (2005) seems to support our proposed age model and allows a tentative definition of the substages MIS 5a, 5c and 5e (Fig. 3). However, one should keep in mind that the relation between these parameters is not fully understood so far and that other factors, such as post-depositional diagenesis, might have an impact on magnetic grain size fluctuations (Xuan et al., 2012).

6.2. Organic carbon accumulation at the Yermak Plateau related to sea ice – ice sheet coupling

Distinct layers rich in terrigenous OC have been traced in cores

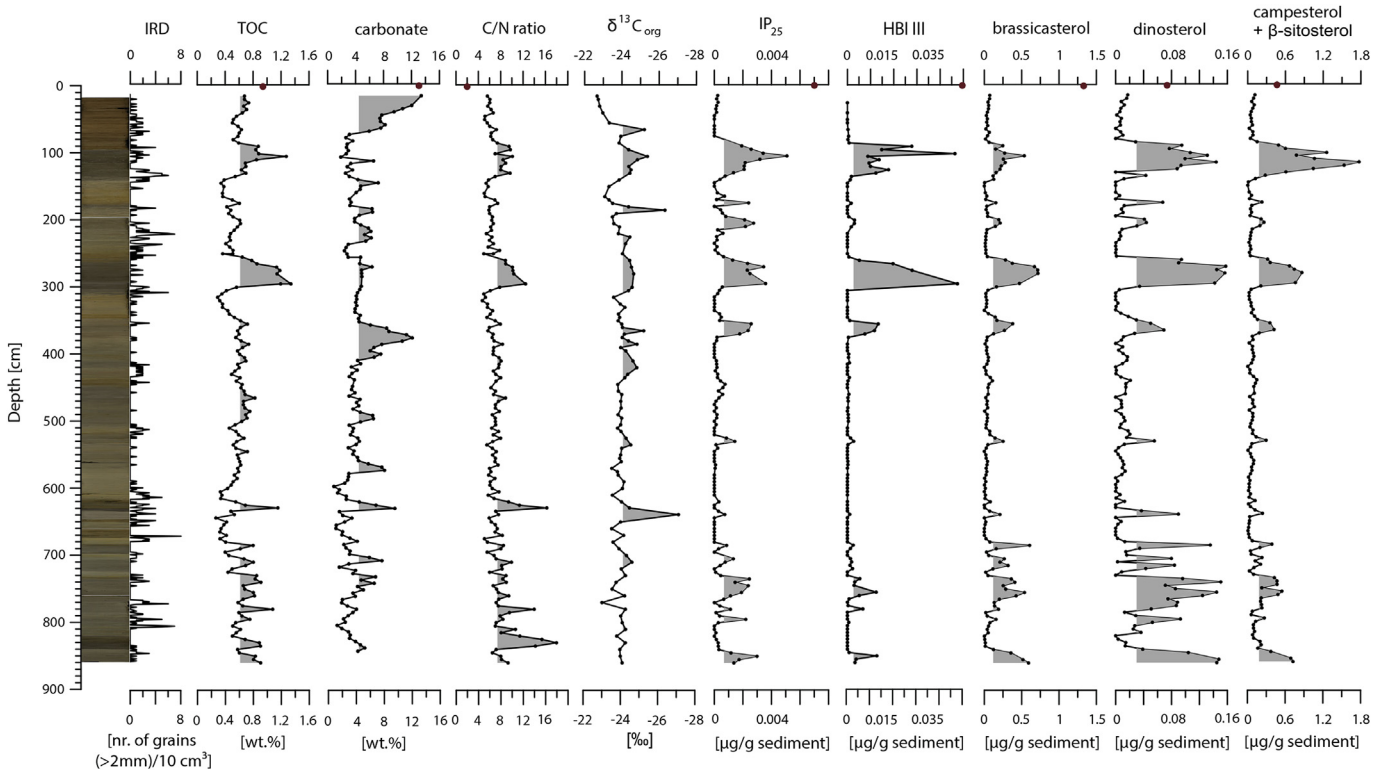

Fig. 2. Line-scan image, bulk parameter contents (IRD [nr. of grains (>2 mm)/10 cm^3], TOC [wt.%], carbonate [wt.%], C/N ratio, $\delta^{13}C_{org}$ [‰]) and biomarker contents (IP_{25} [µg/g sediment], HBI III [µg/g sediment], brassicasterol [µg/g sediment], dinosterol [µg/g sediment], sum of terrigenous sterols: campesterol and β-sitosterol [µg/g sediment]) of Core PS92/039-2 and Core PS92/039-3 (surface sample, red dot) against depth [cm]. Note that brassicasterol and dinosterol are moving synchronously and that brassicasterol is henceforth used as representative for the phytoplankton sterols. Grey shading highlights values lying above the mean. (For interpretation of the references to colour in this figure legend, the reader is referred to the Web version of this article.)

Table 2
Results of AMS^{14}C.

Lab-ID	Depth [cmbsf]	Material	Corrected Ages, ^{14}C years	Calibrated Ages
BETA 452275	150	*N.pachyderma* sin.	28240 ± 140 BP	29589
BETA 425247	227.5	*N.pachyderma* sin.	38550 ± 520 BP	40367
NTUAMS-3357	298	*N.pachyderma* sin.	44187 ± 2900 BP	44782

Radiocarbon dates were corrected for a reservoir effect of 400 years (Stuiver and Braziunas, 1993; Sarnthein and Werner, 2017) and converted to calendar ages (ka) using the CALIB 7.1 calibration program and the "Marine 13″ calibration data set (Stuiver and Reimer, 1993; Reimer et al., 2013).

Table 3
Age fix points of the age model of Core PS92/039-2.

Depth [cmbsf]	Age [cal. ka B.P.]	Marine Isotope Stage	Fix point Origin
65	11.35	1	1
104.5	15.92	2	1
128	17.87	2	1
150	29.59	3	2
227.5	40.37	3	2
298	44.78	3	2
388	81	5.1	3
610	130	5/6 boundary	1

Origin of the age fix points: (1) correlation of carbonate content and magnetic susceptibility to nearby Core PS1533-3 (Spielhagen et al., 2004), (2) AMS radiocarbon dates, (3) occurrence of the benthic foraminifera *Pullenia bulloides*, a stratigraphic marker for event 5.1 (~81 ka) in the polar North Atlantic (Haake and Pflaumann, 1989). Note that AMS14C ages used in the age model of Core PS1533-3 were corrected for a reservoir effect of 400 years and calibrated using the CALIB 4.3 program (Spielhagen et al., 2004) and that the exact ages of the correlation tie points were calculated using linear interpolation. The ages of MIS boundaries are adopted in accordance to Lisiecki and Raymo (2005) and Thompson and Goldstein (2006).

along the northern Eurasian margin of the Arctic Ocean during the late Quaternary (e.g., Elverhøi et al., 1995; Knies and Stein, 1998; Stein et al., 2001; Vogt et al., 2001; Birgel and Stein, 2004; Winkelmann et al., 2008a). Coinciding with episodes of intense glaciation on Svalbard, these intervals were linked to movements of the SBIS. Probable source areas for the terrigenous organic matter are the outcropping OC-rich Mesozoic bedrocks in the northern Barents Sea and on the Spitsbergenbanken (Elverhøi et al., 1989, 1995).

Winkelmann et al. (2008a) investigated this phenomenon in more detail on a series of cores reflecting the paleoceanographic situation of the Sophia Basin north of Svalbard over the last 200 ka. At least five sediment layers possessing similar mineralogical, sedimentological and organic-geochemical features could be correlated and were termed "Terrigenous Input Events" (TIEs). The most striking features of these intervals are enhanced OC contents, elevated C/N ratios, lowest to zero carbonate contents and coarser grain sizes. The chronology of the TIEs was assigned to the onset of the late Saalian glaciation (TIE 4), Termination II (TIE 3), the onset and termination of the Mid Weichselian glaciation (TIE 2), the LGM

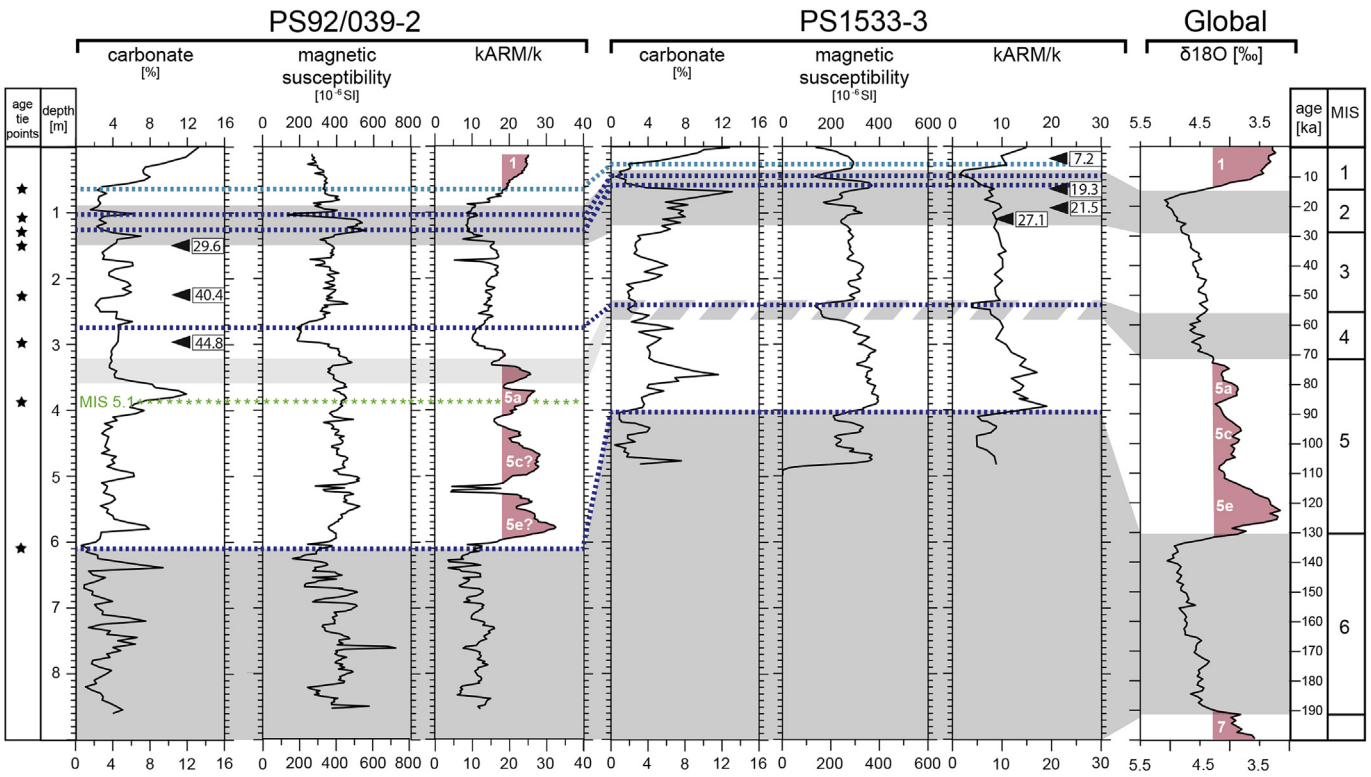

Fig. 3. Stratigraphic framework of Core PS92/039-2. The age tie points (black asterisks) derive from: the correlation of (1) a significant decrease in the carbonate content (light blue, dashed line), (2) a minimum followed by (3) a maximum in the magnetic susceptibility record (blue, dashed lines) to corresponding values at nearby Core PS1533-3 (Spielhagen et al., 2004), (4, 5, 6) radiocarbon ages (indicated as calibrated dates; ka B.P.), (7) the identification of *Pullenia bulloides* as stratigraphic marker for MIS event 5.1 (green asterisks; Haake and Pflaumann, 1989) and (8) a distinct decrease in the magnetic susceptibility correlated to Core PS1533-3 (Spielhagen et al., 2004). An additional, independent confirmation of the age model is given by the correlation of the kARM/k ratio of Core PS92/039-2 to the global benthic $\delta^{18}O$ record of Lisiecki and Raymo (2005). The kARM/k ratio of Core PS1533-3 is indicated for comparability (Nowaczyk et al., 1994). Interglacial minima in the global benthic $\delta^{18}O$ stack are highlighted in red colouration and transferred to the kARM/k ratio of Core PS92/039-2. The ages of MIS boundaries are adopted in accordance to Lisiecki and Raymo (2005) and Thompson and Goldstein (2006) with grey shading referring to glacial intervals. The grey, hatched area indicates the sediment sequence identified as MIS 4 in the original age model of Core PS1533-3 (Spielhagen et al., 2004). The positions of the stage boundaries of MIS 4 in Core PS92/039-2 were calculated using linear interpolation and have to be considered as possible insecurity. (For interpretation of the references to colour in this figure legend, the reader is referred to the Web version of this article.)

(TIE 1) and Termination I (TIE 0). No increased terrigenous input has been observed in connection with the supposed glaciation around 110 ka (Mangerud et al., 1998), suggesting that this phase of ice sheet formation was probably more pronounced at the western continental margin of Svalbard (Winkelmann et al., 2008a).

In Core PS92/039-2 from the eastern Yermak Plateau, three comparable sediment horizons can be identified for the last 160 ka (Fig. 6). According to the high concentration of OC, these horizons are visually conspicuous because of their dark greyish colour (Fig. 2). The predominance of terrigenous OC is indicated by elevated C/N ratios and a tendency to lighter $\delta^{13}C_{org}$ values. Meanwhile, the carbonate content is significantly lowered. In addition to these features that were thoroughly described by previous studies, our biomarker data complete the overall picture of these events with regard to sea ice conditions at that time. All intervals are characterised by peak accumulation rates of the sea ice proxy IP_{25} synchronously with maximum fluxes of the marine biomarkers brassicasterol, dinosterol and HBI III and the landplant-derived sterols campesterol and β-sitosterol (Fig. 2). Hence, conditions must have been favourable for both sea ice and open water algal growth accompanied by a continuous input of terrigenous material. These processes were previously reported as typical features along the ice edge (Smith, 1987; Stein et al., 2016). Terrigenous material is entrapped during the formation of new sea ice in the Kara and Laptev Sea shelf regions, transported via the Transpolar Drift and released at the ice edge due to ablative processes (Reimnitz et al., 1994; Stein et al., 1994). The resulting high-nutrient suspension in the surface water facilitates primary productivity (Sakshaug, 2004). As carbonate dissolution is often enhanced in areas of high productivity and seasonal sea ice formation, this might explain the low carbonate content during these events (Knies, 1994; Steinsund and Hald, 1994). For sea ice diatoms living in/at the underside of the ice, the environmental setting along the ice edge is most favourable due to light and nutrient availability (Fahl and Stein, 2012). Such marginal sea ice conditions are indicated by P_BIP_{25} indices between 0.5 and 0.75 (Fig. 5). The simultaneous input of marine and terrestrial organic matter is further reflected in the $\delta^{13}C_{org}$ signature of these specific layers. Although the predominance of terrigenous organic matter is expressed by a shift towards lighter values, typical terrigenous endmember values around −27‰ (Fernandes and Sicre, 2000) are not reached. Obviously, the concurrent admixture of isotopically enriched phytoplankton (−20‰; Knies et al., 2003) and ice algae (−15 to −8‰; Gibson et al., 1999) alters the $\delta^{13}C_{org}$ signal.

The chronology of the OC events at the Yermak Plateau (PS92/039-2) seems to be connected to major deglaciation intervals on Svalbard (Fig. 6; cf., Winkelmann et al., 2008a). As the SBIS started to retreat after its maximal extensions around 140, 60 and 20 ka, enormous discharges of glacially eroded material took place. Captured by meltwater plumes and dense bottom currents, the reworked material spread along the northern continental margins (Knies and Stein, 1998). The lateral advection of the fine material to

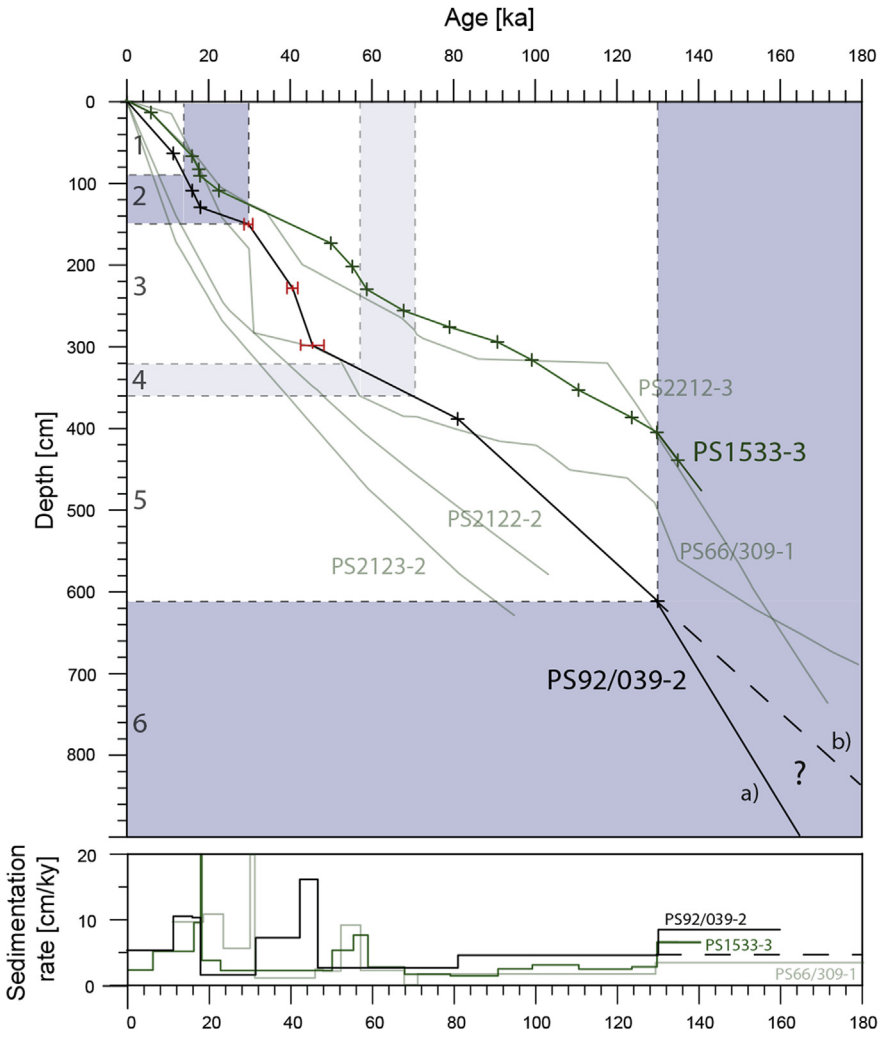

Fig. 4. Age-depth model and sedimentation rates [cm/ky] for the cores PS92/039-2 (black), PS1533-3 (green, green crosses indicate age tie points) and PS2123-3, PS2122-2, PS2212-3, PS66/309-1 (pale print). Calibrated radiocarbon dates with error bars are highlighted in red. Black crosses indicate age tie points obtained from biostratigraphy and correlation of the carbonate and magnetic susceptibility records to nearby Core PS1533-3 (Spielhagen et al., 2004). A linear interpolation is used to calculate ages in between these age tie points. MIS boundaries (according to Lisiecki and Raymo [2005] and Thompson and Goldstein [2006]) are indicated by dashed lines, blue shading refers to glacial intervals. The positions of the stage boundaries for MIS 4 were calculated using a linear interpolation and have to be considered as possible insecurity. According to linear extrapolation, the age of the core base is ~180 ka (option b). However, previous studies north of Spitsbergen described significantly higher sedimentation rates in MIS 6 compared to the following MIS 5 interval (Knies et al., 2001; Stein et al., 2001; Winkelmann et al., 2008a,b). Assuming similar changes for Core PS92/039-2, the more probable age of the core base is ~160 ka (option a). (For interpretation of the references to colour in this figure legend, the reader is referred to the Web version of this article.)

the core site significantly supported the preservation of organic matter released at the nearby ice margin. Knies and Stein (1998) found highest sedimentary contents of marine organic matter in the northern Barents Sea as a result of scavenging on reworked terrigenous particles ("mineral ballast effect"). The formation of aggregates enables an efficient vertical transport through the water column and a subsequent burial at the sea floor (Ittekkot et al., 1992; Knies and Stein, 1998). A more detailed evaluation of the individual events with regard to the predominant paleoceanographic situation is given in the following chapter.

6.3. Sea ice variations at the eastern Yermak Plateau over the last 160 ka

6.3.1. The Saalian (MIS 6; 160–130 ka)

Reconstructions of the QUEEN (Quaternary Environment of the Eurasian North) programme revealed that the Saalian glacial was the most extensive glaciation in northern Eurasia during the late Quaternary (Svendsen et al., 2004). Ice sheets covered the Barents and Kara Seas to the shelf edge and probably the Severnaya Zemlya Archipelago (Polyak et al., 2001; Astakhov, 2004; Jakobsson et al., 2016). On the shelves north of Svalbard, some areas show streamlined patterns on the sea floor in water depths of up to 800 m with a proposed age of the MIS 6 glaciation (e.g., Vogt et al., 1994; Dowdeswell et al., 2010; Jakobsson et al., 2010). Possible explanations for the observed features include the northward expansion of the SBIS onto the Yermak Plateau, the grounding of large fragments of glacial ice, an armada of deep icebergs and the existence of a pan-Arctic ice shelf (Svendsen et al., 2004; Dowdeswell et al., 2010; Jakobsson et al., 2016).

Based on our biomarker records of Core PS92/039-2, there is no indication for an ice sheet covering the northern Yermak Plateau throughout the entire MIS 6. The sea ice proxy IP_{25} fluctuates around mean values of 0.001 μg/g sediment intercalated by short intervals of near zero contents (Fig. 6). Nonetheless, a more or less continuous input can be observed during this interval, indicating seasonally open-water conditions. Simultaneously with enhanced IP_{25} fluxes, increased accumulation of the phytoplankton

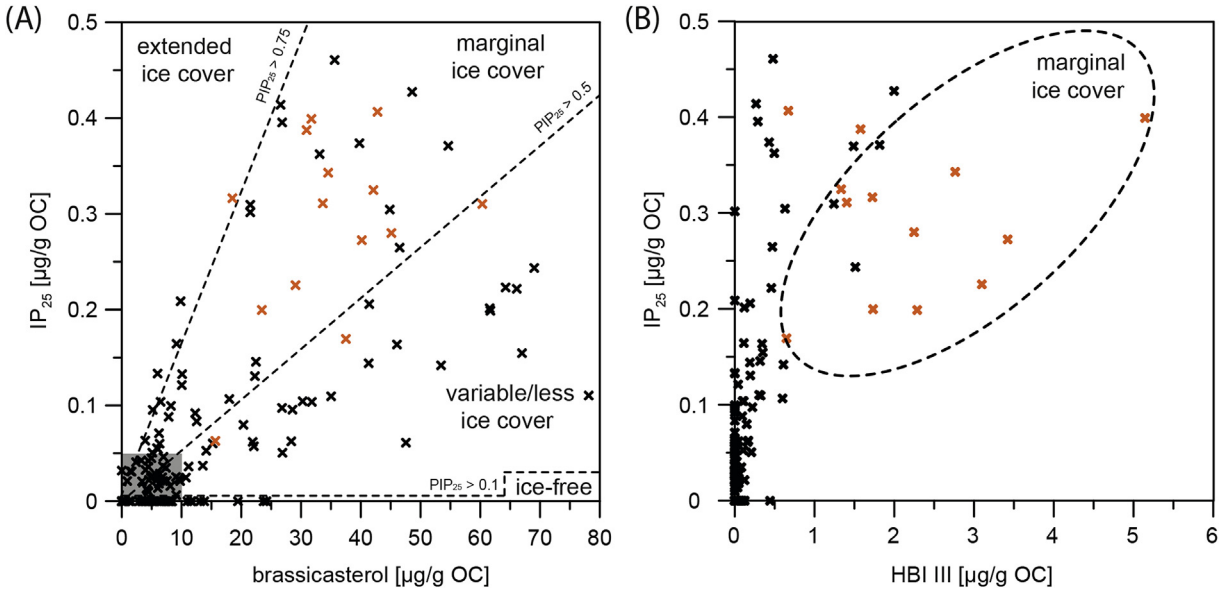

Fig. 5. IP_{25} [µg/g OC] versus (A) brassicasterol [µg/g OC] and (B) HBI III [µg/g OC]. The classification of the different sea ice scenarios refers to Müller et al. (2011). The grey rectangle indicates PIP_{25} values of 1, representative for a permanent sea ice cover. As there is no empirical correlation between the $P_{III}IP_{25}$ index and sea ice conditions so far, a comparable relation was assumed and the categorisation of Müller et al. (2011) adopted. Orange crosses indicate data points from intervals of enhanced organic carbon accumulation on the Yermak Plateau. (For interpretation of the references to colour in this figure legend, the reader is referred to the Web version of this article.)

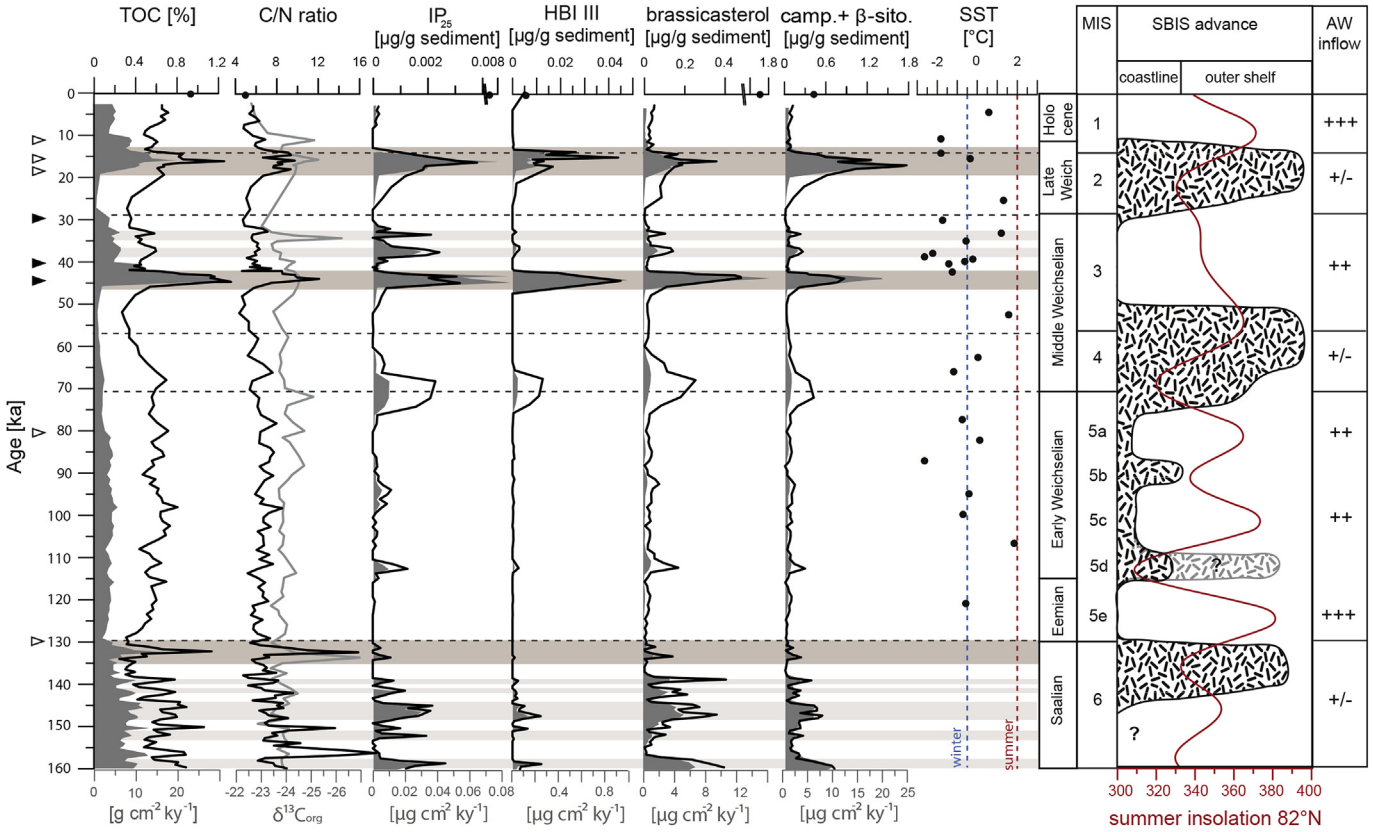

Fig. 6. Fluctuations of the TOC content [wt.%], $\delta^{13}C_{org}$ values [‰], the C/N ratio and the biomarker concentrations [µg/g sediment] against age [ka]. Accumulation rates of TOC [g cm^{-2} ky^{-1}] and the biomarkers [µg cm^{-2} ky^{-1}] are indicated as grey colouration. Note that the core age of ~160 ka is based on the assumption that the change in sedimentation rate between MIS 5 and MIS 6 is similar to observations in adjacent cores (Knies et al., 2001; Stein et al., 2001; Winkelmann et al., 2008a,b). Age tie points are indicated by triangles, filled triangles represent calibrated radiocarbon ages. Brown shading refers to sequences of synchronously enhanced contents of terrigenous organic carbon, IP_{25}, the phytoplankton markers (brassicasterol, HBI III) and the terrigenous sterols (β-sitosterol, campesterol), whereby the darker colour highlights the most conspicuous intervals. OH-GDGT-based SST estimates (after Lü et al., 2015) in the range of −2.5–2.5 °C highlight the throughout close proximity to the sea ice margin. Todays mean summer and winter SSTs in the study area are indicated by dashed red and blue lines, respectively (cf., Sarnthein et al., 2003). On the right side, the summer insolation at 82°N (Laskar et al., 2004), the extent of the Svalbard Barents Sea Ice Sheet (SBIS; Mangerud et al., 1998; Winkelmann et al., 2008a,b) and the inflow strength of Atlantic Water (Spielhagen et al., 2004) are illustrated for the last 160,000 years. (For interpretation of the references to colour in this figure legend, the reader is referred to the Web version of this article.)

(brassicasterol, dinosterol, HBI III) and terrigenous (campesterol, β-sitosterol) biomarkers can be observed during most parts of MIS 6, suggesting the presence of marginal sea ice cover at the Yermak Plateau at that time. A combination of katabatic winds from the protruded SBIS and upwelling of relatively warm AW along its shelf break might have triggered the formation of a coastal polynya along the northern Barents Sea margin (cf., Knies et al., 1999, 2000; Stein et al., 2017b) with the parallel formation of a stationary ice margin at the eastern Yermak Plateau (Fig. 8). A similar MIS 6 scenario is described for the East Siberian continental margin, where the northward extension of the East Siberian Chukchi Ice Sheet (Niessen et al., 2013) probably triggered the formation of a polynya in front of it, enabling ice diatom and phytoplankton production at the southern Lomonosov Ridge (Stein et al., 2017b). Relatively high OC contents of predominantly terrigenous origin (low $\delta^{13}C$ values, high C/N ratios) indicate the input of glacially eroded material along the Eurasian continental margin at that time (Knies et al., 2000, 2001). The distinct variability of the biomarker and the organic-geochemical bulk parameter records may indicate rather unstable oceanographic conditions. The stratification of MIS 6 sediments in Core PS92/039-2 further implies several alterations of the environmental and sedimentary regime (Fig. 2). This means that the sea ice margin may have shifted back and forth several times during MIS 6, probably linked to the glaciation mode of Svalbard. An unstable behaviour of the SBIS, with repeated waxing and waning to the outer shelf, is reported for late MIS 6 as a result of episodically intensified advection of warm AW (Knies et al., 2001; Matthiessen et al., 2001). Similar occasional destabilisation of the ice sheet might have occurred in the course of strengthened AW inflow around 145, 165 and 180 ka (Lloyd et al., 1996; Hebbeln and Wefer, 1997; Wollenburg et al., 2001).

A drop to zero fluxes of IP_{25} and minimum fluxes of the phytoplankton markers as well as related P_BIP_{25} and $P_{III}IP_{25}$ maxima towards the end of MIS 6 indicates the establishment of more severe ice cover at the Yermak Plateau (Fig. 7). The sea ice margin possibly followed the southward migration of the SBIS as the coastal polynya in front of the ice sheet formed back. Now covering the Yermak Plateau with perennial sea ice, any primary production or material release is prohibited (Fig. 8). An alternative explanation might be a short expansion of the SBIS onto the Yermak Plateau. However, the biomarker data allow no differentiation between a perennial sea ice cover and a km-thick ice shelf.

The collapse of major parts of the SBIS after the Penultimate Glacial Maximum around 140 ka (Colleoni et al., 2016) was linked to increasing insolation coupled to strengthened inflow of AW along the western Svalbard Archipelago (Spielhagen et al., 2004). In Core PS92/039-2, peak contents of terrigenous OC (C/N ratio ~15) accompanied by slightly enhanced biomarker abundances may indicate the influence of the distinct meltwater event reconstructed by previous studies around Termination II (Knies et al., 2001; Knies and Vogt, 2003; Spielhagen et al., 2004). Winkelmann et al. (2008a) described increased OC accumulation at times of "Terrigenous Input Event 3". Fed by the thawing ice sheet, such meltwater plumes flow downslope and incorporate fine-grained, mainly terrigenous sediment on the way (cf., Birgel and Hass, 2004). By absorption onto these suspended particles, marine organic matter produced in the nearby MIZ may have been transported to areas covered by perennial sea ice, hence, the Yermak Plateau during that time (Soltwedel et al., 2000; Rutgers van der Loeff et al., 2002).

6.3.2. The Eemian and the early Weichselian (MIS 5; 130–71 ka)

During MIS 5, biomarker concentrations are variable, but among their lowest values in the entire record (Fig. 6). The resulting P_BIP_{25} and $P_{III}IP_{25}$ indices indicate most severe ice conditions with perennial sea ice cover (Fig. 7). The presence of sea ice is further indicated by (summer) SSTs below 2.5 °C (Fig. 6; cf., Sarnthein et al., 2003). The IRD signal is strongly diminished, additionally suggesting a closed ice cover. In contrast to that, previous studies described MIS 5 as a period characterised by SSTs comparable to the recent or even warmer ones (e.g., Matthiessen and Knies, 2001; Matthiessen et al., 2001; Spielhagen et al., 2004; Bauch, 2013). Along the Barents Sea continental margin, the presence of sea ice was significantly reduced, especially during the interstadials MIS 5e, 5c and 5a (Wollenburg et al., 2001; Chauhan et al., 2014; Stein et al., 2017b). However, these observations mainly derive from cores situated directly within the inflow path of AW to the Arctic Ocean. Upwelling of this relatively warm water mass might have triggered the formation of open water areas on the shelves west and north of Svalbard, especially in combination with the insolation maxima around 125, 100 and 80 ka (Laskar et al., 2004). Nonetheless, the more interior parts of the Arctic Ocean remained unaffected (or affected to a lesser degree) by the inflow of warm AW and experienced predominantly permanent ice conditions (Stein et al., 2017b) with the summer sea ice boundary positioned slightly southward of the core position of PS92/039-2 on the eastern Yermak Plateau. However, the abundance of various ichnofossils throughout MIS 5 might indicate occasional nutrient transfer to the seafloor caused by ephemeral break-up of the sea ice cover (Supplementary Fig. 1).

Two phases of moderately enhanced IP_{25} and phytoplankton marker fluxes and resulting lowered P_BIP_{25} and $P_{III}IP_{25}$ indices around 112 and 95 ka indicate phases of reduced sea ice cover. This is further supported by slightly enhanced input of the terrigenous sterols implying a release of material trapped in sea ice due to melting processes. The intervals coincide with distinct insolation minima and might represent the colder substages 5d and 5b (Fig. 6; cf., Laskar et al., 2004). Terrestrial mapping and OSL (optically stimulated luminescence) dating of tills suggest the presence of huge ice sheets covering northern Siberia and the Kara Sea to the shelf edge during the early Weichselian glaciation (MIS 5d-b; Svendsen et al., 2004), coinciding with an extended sea ice cover at the northern Barents Sea continental margin (Stein et al., 2017b). Observations from the western continental margin of Svalbard indicate a major ice sheet advance during substage 5d followed by a less pronounced, more local one during 5b (Mangerud et al., 1996, 1998). In any case, no indication for a major glaciation of the shelf regions northeast of Svalbard could be identified during this period (Knies et al., 1999, 2000, 2001; Winkelmann et al., 2008a). In Core PS92/039-2, the almost constant records of the OC content and the C/N ratio clearly indicate a reduced input of glacially reworked material from the Svalbard region. However, minor northward advances of the SBIS might have triggered ephemeral break-up of the permanent ice cover above the Yermak Plateau, permitting some ice diatom and phytoplankton production. These intervals of seasonally open water are further recorded by moderate IRD input. However, the age control within MIS 5 needs to be improved in order to interpret the paleoceanographic situation in more detail.

6.3.3. The middle Weichselian (MIS 4 and 3; 71–29 ka)

An interval of enhanced AW inflow is recorded in cores along the northern Barents Sea continental margin for late MIS 5 and early MIS 4 (e.g., Matthiessen and Knies, 2001; Wollenburg et al., 2001; Chauhan et al., 2014). It is suggested that the resulting open-water areas in the Nordic Seas and parts of the Arctic Ocean acted as essential moisture sources for the subsequent ice sheet growth initiated by declining insolation (minimum around 72 ka; Laskar et al., 2004). Spielhagen et al. (2004) even claimed an "optimum combination" of AW intrusion (moisture supply) and climatic conditions (temperature and pressure gradients) for MIS 4, leading to fast glaciation of northern Eurasia. First evidence for an

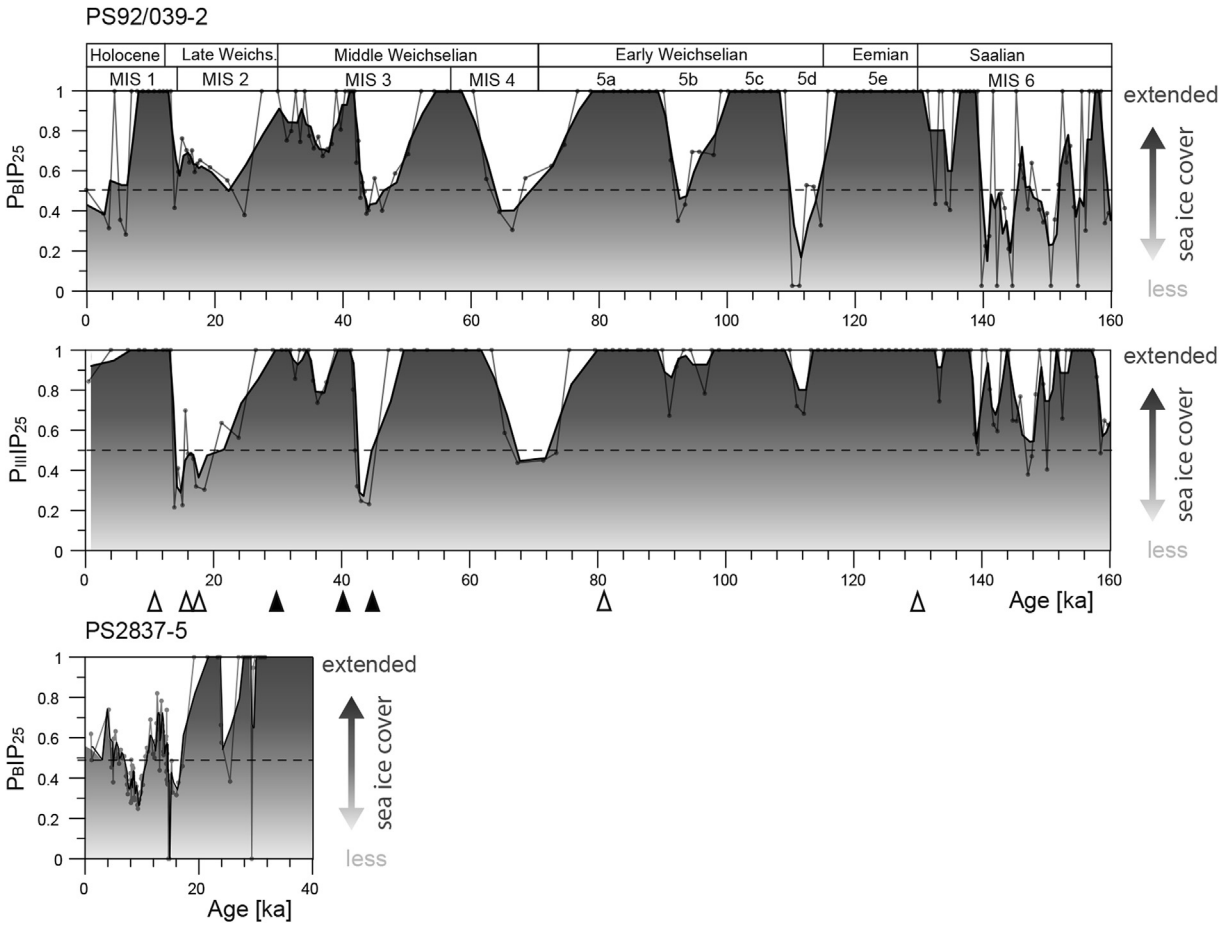

Fig. 7. PIP_{25} indices for Core PS92/039-2 from the eastern Yermak Plateau over the last 160,000 years. Note that the core age of ~160 ka is based on the assumption that the change in sedimentation rate between MIS 5 and MIS 6 is similar to observations in adjacent cores (Knies et al., 2001; Stein et al., 2001; Winkelmann et al., 2008a,b). P_BIP_{25} indices are calculated using the sterol brassicasterol as phytoplankton marker, while $P_{III}IP_{25}$ indices include the tri-unsaturated HBI III as open water counterpart. The coloured area displays the floating average of three data points. The classification of the different sea ice scenarios refers to Müller et al. (2011), whereby the dark to light grey shading indicates the transition from extended to less sea ice cover. As there is no empirical correlation between the $P_{III}IP_{25}$ index and sea ice conditions so far, a comparable relation was assumed and the categorisation of Müller et al. (2011) adopted. Age tie points are indicated by triangles, filled triangles represent calibrated radiocarbon ages. For the last 40 ka, a comparison with P_BIP_{25} indices for Core PS2837-5 from the western Yermak Plateau is given (Müller et al., 2009).

ice sheet advance on Svalbard is reflected in the IRD records from Core PS2138-1 between 75 and 70 ka (Knies et al., 2000, 2001). Coevally, ice diatom and phytoplankton production increased at the Yermak Plateau, indicated by rising sedimentary abundances of IP_{25}, brassicasterol and HBI III in Core PS92/039-2. Higher fluxes likely occurred as a result of reduced ice thickness, hence better light penetration and nutrient availability. As these enhanced abundances are also reflected in the content of the terrigenous biomarkers, the establishment of a stationary sea ice margin above the Yermak Plateau seems to accompany the MIS 5/4 transition. This is also in accordance with a decrease in the P_BIP_{25} and $P_{III}IP_{25}$ indices indicating less severe and probably marginal sea ice cover. Similar to MIS 6, the formation of a coastal polynya in front of the protruding ice sheet might have led to a northward shift of the sea ice margin. However, no enhanced input of glacially eroded material from Svalbard is evident in Core PS92/039-2 at that time (TOC ~0.6%, C/N ratio ~8; Fig. 6). As already suggested by other studies from the region, a more restricted ice sheet expansion during MIS 4 is likely. The greater distance of the ice shelf edge is also indicated by lower bulk accumulation rates compared to the glacial MIS 6 and 2 (Fig. 6; Knies et al., 2000). Hence, the intensive intrusion of AW in early MIS 4 might have been more decisive for the formation of wide ice-free areas north of Svalbard than the extent of the SBIS. As the inflow weakens, the sea ice cover rapidly thickens, marked by a sudden drop of biomarker concentrations around 67 ka. Near zero biomarker and OC fluxes highlight the presence of a permanent ice cover at the Yermak Plateau until 50 ka, inhibiting primary production and the release of terrigenous material.

Exceptionally high accumulation rates of the sea ice proxy IP_{25}, OC and marine and terrigenous sterols reveal an enormous material discharge between 50 and 42 ka. A distinct rise in the C/N ratio highlights the predominantly terrigenous origin of the organic matter.

Previous studies associated early MIS 3 with a series of meltwater events (Mangerud et al., 1998; Knies et al., 2000; Chauhan et al., 2014), probably steered by the northward breakthrough of huge meltwater lakes in the Siberian hinterland (Spielhagen et al., 2004). Fine-grained sediments were flushed off the shelf areas of the Kara and Barents Seas by huge meltwater plumes and laterally advected to the core site at the Yermak slope. The resulting high sedimentary fluxes probably promoted the burial and preservation of material released at the nearby ice margin (Knies and Stein, 1998). Creating a stratified water column with a thick freshwater layer on the surface, this outburst would have encouraged the formation of new sea ice and, in turn, delayed the deglaciation due to a significant cooling of the ocean triggered by positive ice albedo

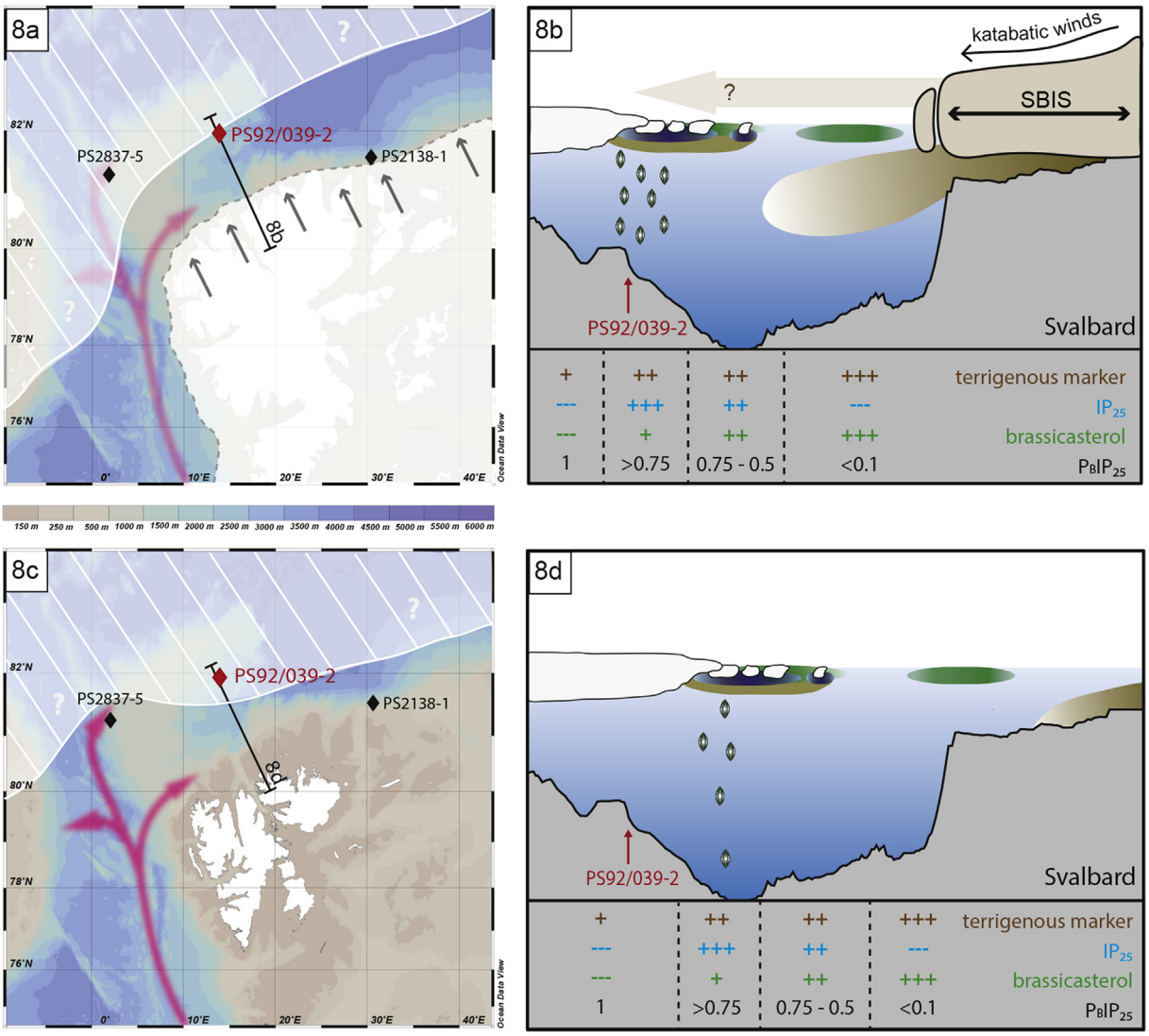

Fig. 8. Overview map and schematic illustration of the sedimentation regime along a transect from the northern coast of Svalbard to the Yermak Plateau (black line) for different settings: (8a, b) scenario for full glacial conditions with major glaciation on Svalbard and (8c, d) scenario for interglacial conditions with no glaciation on Svalbard. The core position of Core PS92/039-2 is indicated in red. The white shading in 8a refers to the extent of the Svalbard Barents Sea Ice Sheet (SBIS), the white crosshatched shading indicates the potential sea ice extent. The thick, light arrow in 8b illustrates the hypothesised advance of the SBIS during MIS 6 that could not be unambiguously identified in the biomarker records of PS92/039-2. Red arrows indicate Atlantic Water entering the Arctic Ocean via the Fram Strait. Blue, green and brown shadings in 8b and 8d mark the input of ice algae, open-water phytoplankton and terrigenous material, respectively. The related sedimentary contents of IP_{25}, the phytoplankton markers and the terrigenous markers as well as P_BIP_{25} indices are indicated. (For interpretation of the references to colour in this figure legend, the reader is referred to the Web version of this article.)

feedback mechanisms (Ruddiman and McIntyre, 1981). Indeed, late MIS 3 is characterised by more severe ice conditions above the Yermak Plateau, indicated by P_BIP_{25} indices mostly between 0.7 and 1 (Fig. 7). The general close proximity to the sea ice margin seems to be supported by SSTs between −2.5 and 2.5 °C (Fig. 6; cf., Sarnthein et al., 2003). Two sequences of slightly enhanced fluxes of OC as well as sea ice, phytoplankton and terrigenous biomarkers can be observed around 38 and 33 ka (Fig. 6). Significantly smaller in amplitude than the event observed around 45 ka, these might reflect a more local influence of the ongoing deglaciation of the Eurasian hinterlands during MIS 3. The continuous input of glacially eroded material along the western continental margin of Svalbard points to a maintenance of minor glaciations on Svalbard prior to the renewed ice sheet growth during latest MIS 3 (Spielhagen, 1991). The trigger for the episodical ice sheet disintegration might be associated with intervals of enhanced inflow of relatively warm AW during MIS 3 (Dokken and Hald, 1996; Hald et al., 2001). These so-called "Nordway Events" (Hebbeln and Wefer, 1997) are characterised by increased biological productivity and thus open water conditions in parts of the Nordic Seas and the Fram Strait (Hebbeln et al., 1994; Dokken and Hald, 1996; Rasmussen and Thomsen, 2008a,b). The enhanced sedimentary biomarker abundances in Core PS92/039-2 that might be correlated with these events, imply a close proximity to the highly productive MIZ throughout MIS 3. The material discharge associated with the ice sheet decay on Svalbard probably fostered the burial and preservation of the organic matter produced at the nearby ice edge.

6.3.4. *The late Weichselian and Holocene (MIS 2 and 1; 29–0 ka)*

The variability of sea ice cover at the western Yermak Plateau (i.e., Core PS2837-5; Fig. 1) was studied in detail by Müller et al. (2009) for the last 30 ka. Due to a comparably low sample resolution for this time interval in Core PS92/039-2, only a rough comparison of the two core sites with regard to sea ice conditions is

possible.

For most of the time interval between 30 and 20 ka, near zero contents of IP_{25} and brassicasterol suggest the presence of perennial sea ice at the western Yermak Plateau. This is followed by a gradual rise of IP_{25} and brassicasterol indicating improved conditions for ice diatom and phytoplankton growth. The resulting P_BIP_{25} index reveals the prevalence of seasonal sea ice that continues trough the Holocene (Fig. 7; Müller et al., 2009).

The eastern Yermak Plateau (i.e., Core PS92/039-2), on the other hand, experienced extended sea ice around 30 ka, followed by an interval predominated by marginal sea ice (Fig. 7). Similar to the glaciations during MIS 6 and 4, katabatic winds from the protruding ice sheet and/or strengthened AW intrusion probably led to the formation of a coastal polynya north of Svalbard (Fig. 8). After reaching minimum insolation during the Last Glacial Maximum ~20 ka, the SBIS became more unstable (Knies et al., 2000; Chauhan et al., 2014). Rapid disintegration started around ~15 ka with the onset of the Bølling warm period (Ruddiman and McIntyre, 1981; Fairbanks, 1989; Rasmussen et al., 2002). Coincidently, peak accumulation rates of terrigenous OC, IP_{25} and the phytoplankton markers in Core PS92/039-2 indicate huge material discharge associated with the deglaciation process (Fig. 6). Winkelmann et al. (2008a) described the enhanced lithogenic flux observed in cores along the northern Barents Sea continental margin at that time as "Terrigenous Input Event 0". The final retreat of the ice sheet to the coastline of Svalbard around 13 ka (Landvik et al., 1998; Mangerud et al., 1998; Hughes et al., 2016) apparently resulted in the re-establishment of perennial sea ice at the eastern Yermak Plateau, indicated by a sudden drop of biomarker contents in Core PS92/039-2. Like the western Yermak Plateau, the eastern part experienced seasonal sea ice during the late Holocene, indicated by enhanced biomarker fluxes in Core PS92/039-2 (Fig. 6).

Taken together, the sea ice conditions at both core sites follow a comparable trend with a few discrepancies probably indicating the local environmental forces. Hence, the eastern Yermak Plateau seems to be more strongly influenced by the northward expansion of the SBIS while the western part is likely more impacted by AW that flows along its western flank.

7. Conclusions

Our biomarker-based reconstruction of sea ice conditions at the eastern Yermak Plateau during the last 160 ka reveals novel information about the complex interplay between sea ice and different environmental forces that decisively affect the sedimentation regime throughout glacial-interglacial cycles. Our study suggests that a simplified scenario with more sea ice during glacials and less sea ice during interglacials is not constantly applicable for the study area.

The following statements can be made:

- During glacial intervals, the eastern Yermak Plateau experienced periodically marginal sea ice conditions. The combination of katabatic winds from the protruding SBIS in combination with upwelling of warm Atlantic Water along its shelf edge probably led to the formation of a coastal polynya north of Svalbard with contemporaneous sea ice margin occurrence in the vicinity of the site of Core PS92/039-2.
- An advance of the SBIS onto the Yermak Plateau throughout the (entire) Saalian glaciation can not be supported by our new biomarker data. However, the environment north of Svalbard appeared to be a highly dynamic system during MIS 6 with repeated waxing and waning of the SBIS to the outer shelf and possibly temporary onto the Yermak Plateau.
- Severe, but variable sea ice cover prevailed at the Yermak Plateau during interglacial periods.
- Maximum fluxes of OC, IP_{25} and the phytoplankton and terrigenous biomarkers can be observed during deglaciation phases, when meltwater plumes from the disintegrating ice sheets in northern Eurasia spread high amounts of glacially reworked material along the continental margins.
- The comparison of the sea ice variability between the eastern and the western Yermak Plateau over the last 30 ka highlights the regional impact of different environmental forces like ice sheet extent and Atlantic Water inflow.

Acknowledgements

We thank the captain and the crew of R/V Polarstern for excellent cooperation during the TRANSSIZ cruise PS92 (grant-no. AWI_PS92_00) in 2015. Thanks to W. Luttmer for technical support during the laboratory work and to Ingrid L. Olsen and Sigrun Hegstad for supporting the acquisition of the line-scan images. Thanks to Simon Belt and colleagues (Biogeochemistry Research Centre, University of Plymouth) for providing the internal standard for the IP_{25} analyses. The paper is a contribution to the German-Chinese project with the title "Natural variability of Arctic sea ice and its significance for global climate change and OC cycle". Financial support was given by the Federal Ministry of Education and Research (BMBF, project-no. 01DO14004), the National Natural Science Foundation of China (project-no. 41406217) and by the Swedish Research Council (grant no. 2014-4108). The authors would like to thank the editor and two anonymous reviewers for their thorough and helpful comments to improve the manuscript.

Appendix A. Supplementary data

Supplementary data related to this article can be found at https://doi.org/10.1016/j.quascirev.2017.12.016.

References

Aagaard, K., 1982. Inflow from the Atlantic ocean to the polar basin. In: Rey, L. (Ed.), The Arctic Ocean. Comité Arctique International, Monaco, pp. 69–82.
Aagaard, K., Foldvik, A., Hillman, S.R., 1987. The West Spitsbergen current - disposition and water mass transformation. J. Geophys. Res.: Oceans 92, 3778–3784.
Aagaard, K., Coachman, L., 1968. The East Greenland Current North of Denmark Strait: Part II. Arctic, vol. 21, pp. 181–200.
Astakhov, V., 2004. Middle Pleistocene glaciations of the Russian north. Quat. Sci. Rev. 23, 1285–1311.
Bauch, H.A., 2013. Interglacial climates and the Atlantic meridional overturning circulation: is there an Arctic controversy? Quat. Sci. Rev. 63, 1–22.
Belt, S.T., Allard, W.G., Massé, G., Robert, J.M., Rowland, S.J., 2000. Highly branched isoprenoids (HBIs): identification of the most common and abundant sedimentary isomers. Geochem. Cosmochim. Acta 64, 3839–3851.
Belt, S.T., Massé, G., Rowland, S.J., Poulin, M., Michel, C., LeBlanc, B., 2007. A novel chemical fossil of palaeo sea ice: IP_{25}. Org. Geochem. 38, 16–27.
Belt, S.T., Massé, G., Vare, L.L., Rowland, S.J., Poulin, M., Sicre, M.-A., Sampei, M., Fortier, L., 2008. Distinctive ^{13}C isotopic signature distinguishes a novel sea ice biomarker in Arctic sediments and sediment traps. Mar. Chem. 112, 158–167.
Belt, S.T., Cabedo-Sanz, P., Smik, L., Navarro-Rodriguez, A., Berben, S.M.P., Knies, J., Husum, K., 2015. Identification of paleo Arctic winter sea ice limits and the marginal ice zone: optimised biomarker-based reconstructions of late Quaternary Arctic sea ice. Earth Planet Sci. Lett. 431, 127–139.
Belt, S.T., Müller, J., 2013. The Arctic sea ice biomarker IP_{25}: a review of current understanding, recommendations for future research and applications in palaeo sea ice reconstructions. Quat. Sci. Rev. 79, 9–25.
Berben, S.M.P., Husum, K., Navarro-Rodriguez, A., Belt, S.T., Aagaard-Sørensen, S., 2017. Semi-quantitative reconstruction of early to late Holocene spring and summer sea ice conditions in the northern Barents Sea. J. Quat. Sci. 32, 587–603.
Birgel, D., Hass, H.C., 2004. Oceanic and atmospheric variations during the last deglaciation in the Fram Strait (Arctic Ocean): a coupled high-resolution organic-geochemical and sedimentological study. Quat. Sci. Rev. 23, 29–47.
Birgel, D., Stein, R., 2004. Northern Fram Strait and Yermak Plateau: distribution, variability and burial of organic carbon and paleoenvironmental implications. In: Stein, R., Macdonald, R.W. (Eds.), The Organic Carbon Cycle in the Arctic

Ocean. Springer-Verlag, Berlin, pp, pp. 279–294.
Boon, J.J., Rijpstra, W.I.C., Delange, F., Deleeuw, J.W., Yoshioka, M., Shimizu, Y., 1979. Black sea sterol - molecular fossil for dinoflagellate blooms. Nature 277, 125–127.
Bourke, R., Weigel, A., Paquette, R., 1988. The westward turning branch of the West Spitsbergen Current. J. Geophys. Res.: Oceans 93, 14065–14077.
Brassell, S.C., Eglinton, G., Marlowe, I.T., Pflaumann, U., Sarntheim, M., 1986. Molecular stratigraphy: a new tool for climate assessment. Nature 320, 129–133.
Broecker, W.S., 1997. Thermohaline circulation, the Achilles heel of our climate system: will man-made CO_2 upset the current balance? Science 278, 1582–1588.
Brown, T., Belt, S., Tatarek, A., Mundy, C., 2014. Source identification of the Arctic sea ice proxy IP_{25}. Nat. Commun. 5, 4197.
Brown, T.A., Belt, S.T., 2016. Novel tri- and tetra-unsaturated highly branched isoprenoid (HBI) alkenes from the marine diatom Pleurosigma intermedium. Org. Geochem. 91, 120–122.
Chauhan, T., Rasmussen, T.L., Noormets, R., Jakobsson, M., Hogan, K.A., 2014. Glacial history and paleoceanography of the southern Yermak Plateau since 132 ka BP. Quat. Sci. Rev. 92, 155–169.
Clark, P.U., Dyke, A.S., Shakun, J.D., Carlson, A.E., Clark, J., Wohlfarth, B., Mitrovica, J.X., Hostetler, S.W., McCabe, A.M., 2009. The last glacial maximum. Science 325, 710–714.
Coachman, L.K., Aagaard, K., 1974. Physical Oceanography of Arctic and subarctic seas. In: Herman, Y. (Ed.), Marine Geology and Oceanography of the Arctic Seas. Springer, Berlin, Heidelberg, pp. 1–72.
Colleoni, F., Wekerle, C., Naslund, J.O., Brandefelt, J., Masina, S., 2016. Constraint on the penultimate glacial maximum Northern Hemisphere ice topography (approximate to 140 kyrs BP). Quat. Sci. Rev. 137, 97–112.
Comiso, J.C., Parkinson, C.L., Gersten, R., Stock, L., 2008. Accelerated decline in the Arctic sea ice cover. Geophys. Res. Lett. 35, L01703.
Dieckmann, G.S., Hellmer, H.H., 2008. The importance of sea ice: an overview. In: Thomas, D.N., Diekmann, G.S. (Eds.), Sea Ice: an Introduction to its Physics, Chemistry, Biology, and Geology. Blackwell Science, Oxford, pp. 1–21.
Dokken, T.M., Hald, M., 1996. Rapid climatic shifts during isotope stages 2-4 in the Polar North Atlantic. Geology 24, 599–602.
Dowdeswell, J.A., Jakobsson, M., Hogan, K.A., O'Regan, M., Backman, J., Evans, J., Hell, B., Löwemark, L., Marcussen, C., Noormets, R., Cofaigh, C.O., Sellen, E., Solvsten, M., 2010. High-resolution geophysical observations of the Yermak Plateau and northern Svalbard margin: implications for ice-sheet grounding and deep-keeled icebergs. Quat. Sci. Rev. 29, 3518–3531.
Eglinton, T.I., Eglinton, G., 2008. Molecular proxies for paleoclimatology. Earth Planet Sci. Lett. 275, 1–16.
Elverhøi, A., Pfirman, S.L., Solheim, A., Larssen, B.B., 1989. Glaciomarine sedimentation in epicontinental seas exemplified by the northern Barents sea. Mar. Geol. 85, 225–250.
Elverhøi, A., Svendsen, J.I., Solheim, A., Andersen, E.S., Milliman, J., Mangerud, J., Hooke, R.L., 1995. Late Quaternary sediment yield from the high Arctic Svalbard area. J. Geol. 103, 1–17.
Fahl, K., Stein, R., Gaye-Haake, B., Gebhardt, C., Kodina, L.A., Unger, D., Ittekkot, V., 2003. Biomarkers in surface sediments from the Ob and Yenisei estuaries and southern Kara Sea: evidence for particulate organic carbon sources, pathways, and degradation. In: Stein, R., Fahl, K., Fütterer, D.K., Galimov, E.M., Stepanets, O.V. (Eds.), Siberian River Run-off in the Kara Sea: Characterisation, Quantification, Variability, and Environmental Significance. Proceedings in Marine Sciences, vol. 6. Elsevier, Amsterdam, pp. 329–348.
Fahl, K., Stein, R., 2007. Biomarker records, organic carbon accumulation, and river discharge in the Holocene southern Kara Sea (Arctic Ocean). Geo Mar. Lett. 27, 13–25.
Fahl, K., Stein, R., 2012. Modern seasonal variability and deglacial/Holocene change of central Arctic Ocean sea-ice cover: new insights from biomarker proxy records. Earth Planet Sci. Lett. 351, 123–133.
Fairbanks, R.G., 1989. A 17,000-year Glacio-eustatic sea-level record - influence of glacial melting rates on the younger dryas event and deep-ocean circulation. Nature 342, 637–642.
Fernandes, M.B., Sicre, M.A., 2000. The importance of terrestrial organic carbon inputs on Kara Sea shelves as revealed by n-alkanes, OC and $\delta^{13}C$ values. Org. Geochem. 31, 363–374.
Fietz, S., Huguet, C., Rueda, G., Hambach, B., Rosell-Mele, A., 2013. Hydroxylated isoprenoidal GDGTs in the Nordic seas. Mar. Chem. 152, 1–10.
Gibson, J.A.E., Trull, T., Nichols, P.D., Summons, R.E., McMinn, A., 1999. Sedimentation of ^{13}C- rich organic matter from Antarctic sea-ice algae: a potential indicator of past sea-ice extent. Geology 27, 331–334.
Haake, F.W., Pflaumann, U., 1989. Late pleistocene foraminiferal stratigraphy on the Vøring plateau, Norwegian sea. Boreas 18, 343–356.
Hald, M., Dokken, T., Mikalsen, G., 2001. Abrupt climatic change during the last interglacial- glacial cycle in the polar North Atlantic. Mar. Geol. 176, 121–137.
Hall, A., 2004. The role of surface albedo feedback in climate. J. Clim. 17, 1550–1568.
Haugan, P.M., 1999. Structure and heat content of the west Spitsbergen current. Polar Res. 18 (2), 183–188.
Hebbeln, D., Dokken, T., Andersen, E.S., Hald, M., Elverhøi, A., 1994. Moisture supply for northern ice-sheet growth during the Last Glacial Maximum. Nature 370, 357–359.
Hebbeln, D., Wefer, G., 1997. Late quaternary paleoceanography in the Fram Strait. Paleoceanography 12, 65–78.
Henrich, R., 1998. Dynamics of Atlantic water advection to the Norwegian-Greenland Sea - time- slice record of carbonate distribution in the last 300 ky. Mar. Geol. 145, 95–131.
Ho, S.L., Mollenhauer, G., Fietz, S., Martinez-Garcia, A., Lamy, F., Rueda, G., Schipper, K., Meheust, M., Rosell-Mele, A., Stein, R., Tiedemann, R., 2014. Appraisal of TEX86 and TEX_{86}^{L} thermometries in subpolar and polar regions. Geochem. Cosmochim. Acta 131, 213–226.
Hörner, T., Stein, R., Fahl, K., Birgel, D., 2016. Post-glacial variability of sea ice cover, river run- off and biological production in the western Laptev Sea (Arctic Ocean) - a high-resolution biomarker study. Quat. Sci. Rev. 143, 133–149.
Huang, W.Y., Meinschein, W.G., 1979. Sterols as ecological indicators. Geochem. Cosmochim. Acta 43 (5), 739–745.
Hughes, A.L.C., Gyllencreutz, R., Lohne, Ø.S., Mangerud, J., Svendsen, J.I., 2016. The last Eurasian ice sheets – a chronological database and time-slice reconstruction, DATED-1. Boreas 45, 1–45.
Ingólfsson, Ó., Landvik, J.Y., 2013. The Svalbard-Barents Sea ice-sheet - historical, current and future perspectives. Quat. Sci. Rev. 64, 33–60.
Ittekkot, V., Haake, B., Bartsch, M., Nair, R.R., Ramaswamy, V., 1992. Organic carbon removal in the sea: the continental connection. In: Prell, W.L., Emeis, K.C., Summerhayes, C.P. (Eds.), Upwelling Systems: Evolution since the Early Miocene, vol. 64. Geological Society of London, pp. 167–176. Special Publication.
Ivanov, V.V., Alexeev, V.A., Repina, I., Koldunov, N.V., Smirnov, A., 2012. Tracing Atlantic water signature in the Arctic sea ice cover east of Svalbard. Adv. Microbiol. 2012, 11.
Jaffé, R., Wolff, G.A., Cabrera, A.C., Carvajal-Chitty, H., 1995. The biogeochemistry of lipids in rivers of the Orinoco Basin. Geochem. Cosmochim. Acta 59, 4507–4522.
Jakobsson, M., Nilsson, J., O'Regan, M., Backman, J., Löwemark, L., Dowdeswell, J.A., Mayer, L., Polyak, L., Colleoni, F., Anderson, L., Björk, G., Darby, D., Eriksson, B., Hanslik, D., Hell, B., Marcussen, C., Sellen, E., Wallin, A.., 2010. An Arctic Ocean ice shelf during MIS 6 constrained by new geophysical and geological data. Quat. Sci. Rev. 29, 3505–3517.
Jakobsson, M., Nilsson, J., Anderson, L., Backman, J., Bjork, G., Cronin, T.M., Kirchner, N., Koshurnikov, A., Mayer, L., Noormets, R., O'Regan, M., Stranne, C., Ananiev, R., Macho, N.B., Cherniykh, D., Coxall, H., Eriksson, B., Floden, T., Gemery, L., Gustafsson, O., Jerram, K., Johansson, C., Khortov, A., Mohammad, R., Semiletov, I., 2016. Evidence for an ice shelf covering the central Arctic Ocean during the penultimate glaciation. Nat. Commun. 7, 10365.
Jessen, S.P., Rasmussen, T.L., Nielsen, T., Solheim, A., 2010. A new Late Weichselian and Holocene marine chronology for the western Svalbard slope 30,000-0 cal years BP. Quat. Sci. Rev. 29, 1301–1312.
Kim, J.H., Schouten, S., Hopmans, E.C., Donner, B., Damste, J.S.S., 2008. Global sediment core-top calibration of the TEX_{86} paleothermometer in the ocean. Geochem. Cosmochim. Acta 72, 1154–1173.
Kim, J.H., van der Meer, J., Schouten, S., Helmke, P., Willmott, V., Sangiorgi, F., Koc, N., Hopmans, E.C., Damste, J.S.S., 2010. New indices and calibrations derived from the distribution of crenarchaeal isoprenoid tetraether lipids: implications for past sea surface temperature reconstructions. Geochem. Cosmochim. Acta 74, 4639–4654.
King, J., Banerjee, S.K., Marvin, J., Özdemir, Ö., 1982. A comparison of different magnetic methods for determining the relative grain size of magnetite in natural materials: some results from lake sediments. Earth Planet Sci. Lett. 59 (2), 404–419.
Knies, J., 1994. Spätquartäre Sedimentation Am Kontinentalhang Nordwestlich Spitzbergens. Der Letzte Glazial/Interglazial-zyklus, vol. 95. Justus-Liebig-Universität, Gießen (unpublished diploma thesis).
Knies, J., Vogt, C., Stein, R., 1999. Late Quaternary growth and decay of the Svalbard/Barents Sea ice sheet and paleoceanographic evolution in the adjacent Arctic Ocean. Geo Mar. Lett. 18, 195–202.
Knies, J., Nowaczyk, N., Müller, C., Vogt, C., Stein, R., 2000. A multiproxy approach to reconstruct the environmental changes along the Eurasian continental margin over the last 150 000 years. Mar. Geol. 163, 317–344.
Knies, J., Kleiber, H.-P., Matthiessen, J., Müller, C., Nowaczyk, N., 2001. Marine ice-rafted debris records constrain maximum extent of Saalian and Weichselian ice-sheets along the northern Eurasian margin. Global Planet. Change 31, 45–64.
Knies, J., Hald, M., Ebbesen, H., Mann, U., Vogt, C., 2003. A deglacial-middle Holocene record of biogenic sedimentation and paleoproductivity changes from the northern Norwegian continental shelf. Paleoceanography 18, 1096.
Knies, J., Matthiessen, J., Vogt, C., Laberg, J.S., Hjelstuen, B.O., Smelror, M., Larsen, E., Andreassen, K., Eidvin, T., Vorren, T.O., 2009. The Plio-Pleistocene glaciation of the Barents Sea-Svalbard region: a new model based on revised chronostratigraphy. Quat. Sci. Rev. 28, 812–829.
Knies, J., Stein, R., 1998. New aspects of organic carbon deposition and its paleoceanographic implications along the northern Barents Sea margin during the last 30,000 years. Paleoceanography 13, 384–394.
Knies, J., Vogt, C., 2003. Freshwater pulses in the eastern Arctic Ocean during Saalian and early Weichselian ice-sheet collapse. Quat. Res. 60, 243–251.
Landvik, J.Y., Bondevik, S., Elverhøi, A., Fjeldskaar, W., Mangerud, J., Salvigsen, O., Siegert, M.J., Svendsen, J.I., Vorren, T.O., 1998. The last glacial maximum of Svalbard and the Barents Sea area: ice sheet extent and configuration. Quat. Sci. Rev. 17, 43–75.
Landvik, J.Y., Brook, E.J., Gualtieri, L., Linge, H., Raisbeck, G., Salvigsen, O., Yiou, F., 2013. ^{10}Be exposure age constraints on the Late Weichselian ice-sheet geometry and dynamics in inter-ice-stream areas, western Svalbard. Boreas 42, 43–56.
Laskar, J., Robutel, P., Joutel, F., Gastineau, M., Correia, A., Levrard, B., 2004. A long-

term numerical solution for the insolation quantities of the Earth. Astron. Astrophys. 428, 261–285.
Lisiecki, L.E., Raymo, M.E., 2005. A Pliocene-Pleistocene stack of 57 globally distributed benthic $\delta^{18}O$ records. Paleoceanography 20, PA1003.
Liu, X.L., Summons, R.E., Hinrichs, K.U., 2012. Extending the known range of glycerol ether lipids in the environment: structural assignments based on tandem mass spectral fragmentation patterns. Rapid Commun. Mass Spectrom. 26, 2295–2302.
Lloyd, J.M., Kroon, D., Boulton, G.S., Laban, C., Fallick, A., 1996. Ice rafting history from the Spitsbergen ice cap over the last 200 kyr. Mar. Geol. 131, 103–121.
Lü, X.X., Liu, X.L., Elling, F.J., Yang, H., Xie, S.C., Song, J.M., Li, X.G., Yuan, H.M., Li, N., Hinrichs, K.U., 2015. Hydroxylated isoprenoid GDGTs in Chinese coastal seas and their potential as a paleotemperature proxy for mid-to-low latitude marginal seas. Org. Geochem. 89–90, 31–43.
Mangerud, J., Jansen, E., Landvik, J.Y., 1996. Late Cenozoic history of the Scandinavian and Barents sea ice sheets. Global Planet. Change 12, 11–26.
Mangerud, J., Dokken, T., Hebbeln, D., Heggen, B., Ingólfsson, O., Landvik, J.Y., Mejdahl, V., Svendsen, J.I., Vorren, T.O., 1998. Fluctuations of the Svalbard - Barents sea ice sheet during the last 150 000 years. Quat. Sci. Rev. 17, 11–42.
Manley, T., Bourke, R., Hunkins, K., 1992. Near-surface circulation over the Yermak plateau in northern Fram Strait. J. Mar. Syst. 3, 107–125.
Manley, T., 1995. Branching of Atlantic water within the Greenland-Spitsbergen passage: an estimate of recirculation. J. Geophys. Res.: Oceans 100, 20627–20634.
Matthiessen, J., Knies, J., Nowaczyk, N.R., Stein, R., 2001. Late Quaternary dinoflagellate cyst stratigraphy at the Eurasian continental margin, Arctic Ocean: indications for Atlantic water inflow in the past 150,000 years. Global Planet. Change 31, 65–86.
Matthiessen, J., Knies, J., 2001. Dinoflagellate cyst evidence for warm interglacial conditions at the northern Barents Sea margin, during marine isotope stage 5. J. Quat. Sci. 16, 727–737.
Meyers, P.A., 1997. Organic geochemical proxies of paleoceanographic, paleolimnologic and paleoclimatic processes. Org. Geochem. 27, 213–250.
Müller, J., Massé, G., Stein, R., Belt, S.T., 2009. Variability of sea-ice conditions in the Fram Strait over the past 30,000 years. Nat. Geosci. 2, 772–776.
Müller, J., Wagner, A., Fahl, K., Stein, R., Prange, M., Lohmann, G., 2011. Towards quantitative sea ice reconstructions in the northern North Atlantic: a combined biomarker and numerical modelling approach. Earth Planet Sci. Lett. 306, 137–148.
Müller, J., Werner, K., Stein, R., Fahl, K., Moros, M., Jansen, E., 2012. Holocene cooling culminates in sea ice oscillations in Fram Strait. Quat. Sci. Rev. 47, 1–14.
Müller, J., Stein, R., 2014. High-resolution record of late glacial and deglacial sea ice changes in Fram Strait corroborates ice-ocean interactions during abrupt climate shifts. Earth Planet Sci. Lett. 403, 446–455.
Navarro-Rodriguez, A., Belt, S.T., Knies, J., Brown, T.A., 2013. Mapping recent sea ice conditions in the Barents Sea using the proxy for palaeo sea ice reconstructions. Quat. Sci. Rev. 79, 26–39.
Niessen, F., Hong, J.K., Hegewald, A., Matthiessen, J., Stein, R., Kim, H., Kim, S., Jensen, L., Jokat, W., Nam, S.I., Kang, S.H., 2013. Repeated pleistocene glaciation of the east Siberian continental margin. Nat. Geosci. 6, 842–846.
Nowaczyk, N.R., Frederichs, T.W., Eisenhauer, A., Gard, G., 1994. Magnetostratigraphic data from late quaternary sediments from the Yermak plateau, Arctic-ocean - evidence for 4 geomagnetic polarity events within the last 170 Ka of the brunhes chron. Geophys. J. Int. 117, 453–471.
O'Regan, M., King, J., Backman, J., Jakobsson, M., Pälike, H., Moran, K., Heil, C., Sakamoto, T., Cronin, T.M., Jordan, R.W., 2008. Constraints on the pleistocene chronology of sediments from the Lomonosov Ridge. Paleoceanography 23, PA1S19.
Parkinson, C.L., Comiso, J.C., 2013. On the 2012 record low Arctic sea ice cover: combined impact of preconditioning and an August storm. Geophys. Res. Lett. 40, 1356–1361.
Peeken, I., 2016. The expedition PS92 of the research vessel POLARSTERN to the Arctic Ocean in 2015. Reports on Polar and Marine Research 694, 153.
Polyak, L., Edwards, M.H., Coakley, B.J., Jakobsson, M., 2001. Ice shelves in the Pleistocene Arctic Ocean inferred from glaciogenic deep-sea bedforms. Nature 410, 453–457.
Prahl, F.G., Wakeham, S.G., 1987. Calibration of unsaturation pattern in long-chain ketone compositions for paleotemperature assessment. Nature 330, 367–369.
Pryce, R.J., 1971. The occurrence of bound, water-soluble squalene, 4,4-dimethyl sterols, 4α- methyl sterols and sterols in leaves of Kalanchoe blossfeldiana. Phytochemistry 10, 1303–1307.
Rasmussen, T.L., Thomsen, E., 2008a. Warm Atlantic surface water inflow to the Nordic seas 34–10 cal. kyr B.P. Paleoceanography 23, PA1201.
Rasmussen, T.L., Thomsen, E., 2008b. Warm Atlantic surface water inflow to the Nordic seas 34 – 10 calibrated ka B.P. Paleoceanography 23, PA1201.
Rasmussen, T.L., Bäckström, D., Heinemeier, J., Klitgaard-Kristen- sen, D., Knutz, P.C., Kuijpers, A., Lassen, S., Thomsen, E., Troelstra, S.R., van Weering, T.C.E., 2002. The Faeroe – shet- land gateway: late quaternary water mass exchange between the Nordic seas and the northeastern Atlantic. Mar. Geol. 188, 165–192.
Reimer, P.J., Bard, E., Bayliss, A., Beck, J.W., Blackwell, P.G., Bronk, R.C., Buck, C.E., Cheng, H., Edwards, R.L., Friedrich, M., 2013. IntCal13 and Marine13 radiocarbon age calibration curves 0–50,000 years cal BP. Radiocarbon 55, 1869–1887.
Reimnitz, E., Dethleff, D., Nürnberg, D., 1994. Contrasts in Arctic shelf sea-ice regimes and some implications - beaufort sea versus Laptev sea. Mar. Geol. 119, 215–225.
Robinson, N., Eglinton, G., Brassell, S.C., Cranwell, P.A., 1984. Dinoflagellate origin for sedimentary 4α-methylsteroids and 5α(*H*)-Stanols. Nature 308, 439–442.
Rontani, J.F., Charrière, B., Sempéré, R., Doxaran, D., Vaultier, F., Vonk, J.E., Volkman, J.K., 2014. Degradation of sterols and terrigenous organic matter in waters of the Mackenzie Shelf, Canadian Arctic. Org. Geochem. 75, 61–73.
Rowland, S.J., Allard, W.G., Belta, S.T., Massae, G., Robert, J.M., Blackburn, S., Frampton, D., Revill, A.T., Volkman, J.K., 2001. Factors influencing the distributions of polyunsaturated terpenoids in the diatom, Rhizosolenia setigera. Phytochemistry 58, 717–728.
Ruddiman, W.F., McIntyre, A., 1981. Oceanic mechanisms for amplification of the 23,000-year ice-volume cycle. Science 212, 617–627.
Rudels, B., Friedrich, H.J., Quadfasel, D., 1999. The Arctic circumpolar boundary current. Deep Sea Res. Part II Top. Stud. Oceanogr. 46, 1023–1062.
Rutgers van der Loeff, M.M., Meyer, R., Rudels, B., Rachor, E., 2002. Resuspension and particle transport in the benthic nepheloid layer in and near Fram Strait in relation to faunal abundance and ^{234}Th depletion. Deep-Sea Res. 149, 1941–1958.
Sachs, J.P., Pahnke, K., Smittenberg, R., Zhang, Z., 2013. Biomarker indicators of past climate. In: Elias, S.A. (Ed.), The Encyclopedia of Quaternary Science. Elsevier, Amsterdam, pp. 775–782.
Sakshaug, E., 2004. Primary and secondary production in the Arctic seas. In: Stein, R., Macdonald, R.W. (Eds.), The Organic Carbon Cycle in the Arctic Ocean. Springer, Berlin, pp. 57–82.
Sarnthein, M., Pflaumann, U., Weinelt, M., 2003. Past extent of sea ice in the northern North Atlantic inferred from foraminiferal paleotemperature estimates. Paleoceanography 18 (2), 25–1-25-8.
Sarnthein, M., Werner, K., 2017. Early Holocene planktic foraminifers record species-specific ^{14}C reservoir ages in Arctic Gateway. Mar. Micropaleontol. 135, 45–55.
Schouten, S., Hopmans, E.C., Schefuß, E., Sinninghe Damsté, J.S., 2002. Distributional variations in marine crenarchaeotal membrane lipids: a new tool for reconstructing ancient sea water temperatures? Earth Planet Sci. Lett. 204, 265–274.
Serreze, M.C., Holland, M.M., Stroeve, J., 2007. Perspectives on the Arctic's shrinking sea ice cover. Science 315, 1533–1536.
Serreze, M.C., Barry, R.G., 2011. Processes and impacts of Arctic amplification: a research synthesis. Global Planet. Change 77, 85–96.
Smik, L., Cabedo-Sanz, P., Belt, S.T., 2016. Semi-quantitative estimates of paleo Arctic sea ice concentration based on source-specific highly branched isoprenoid alkenes: a further development of the PIP_{25} index. Org. Geochem. 92, 63–69.
Smith, W.O., 1987. Phytoplankton dynamics in marginal ice zones. Oceanogr. Mar. Biol. 25, 11–38.
Soltwedel, T., Mokievsky, V., Schewe, I., 2000. Benthic activity and biomass on the Yermak Plateau and in adjacent deep-sea regions northwest of Svalbard. Deep-Sea Res. Part I 47, 1761–1785.
Spielhagen, R.F., 1991. Die Eisdrift in der Framstraße während der letzten 200.000 Jahre, vol. 4. GEOMAR, Kiel, Kiel, p. 133. GEOMAR Report.
Spielhagen, R.F., Baumann, K.H., Erlenkeuser, H., Nowaczyk, N.R., Norgaard-Pedersen, N., Vogt, C., Weiel, D., 2004. Arctic Ocean deep-sea record of northern Eurasian ice sheet history. Quat. Sci. Rev. 23, 1455–1483.
Stein, R., Grobe, H., Wahsner, M., 1994. Organic-carbon, carbonate, and clay mineral distributions in eastern central Arctic-ocean surface sediments. Mar. Geol. 119, 269–285.
Stein, R., Boucsein, B., Fahl, K., Garcia de Oteyza, T., Knies, J., Niessen, F., 2001. Accumulation of particulate organic carbon at the Eurasian continental margin during late Quaternary times: controlling mechanisms and paleoenvironmental significance. Global Planet. Change 31, 87–104.
Stein, R., Fahl, K., Müller, J., 2012. Proxy reconstruction of Arctic Ocean sea ice history: from IRD to IP_{25}. Polarforschung 82, 37–71.
Stein, R., Fahl, K., Schreck, M., Knorr, G., Niessen, F., Forwick, M., Gebhardt, C., Jensen, L., Kaminski, M., Kopf, A., Matthiessen, J., Jokat, W., Lohmann, G., 2016. Evidence for ice- free summers in the late Miocene central Arctic Ocean. Nat. Commun. 7, 1–13.
Stein, R., Fahl, K., Schade, I., Manerung, A., Wassmuth, S., Niessen, F., Nam, S., 2017a. Holocene variability in sea ice cover, primary production, and Pacific-Water inflow and climate change in the Chukchi and East Siberian Seas (Arctic Ocean). J. Quat. Sci. 32, 362–379.
Stein, R., Fahl, K., Gierz, P., Niessen, F., Lohmann, G., 2017b. Arctic Ocean sea ice cover during the penultimate glacial and the last interglacial. Nat. Commun. 8, 373.
Stein, R., Fahl, K., 2013. Biomarker proxy shows potential for studying the entire Quaternary Arctic sea ice history. Org. Geochem. 55, 98–102.
Stein, R., Macdonald, R.W., 2004. Geochemical proxies used for organic carbon source identification in Arctic Ocean sediments. In: Stein, R., Macdonald, R.W. (Eds.), The Organic Carbon Cycle in the Arctic Ocean. Springer-Verlag, Berlin, pp. 24–32.
Steinsund, P.I., Hald, M., 1994. Recent calcium-carbonate dissolution in the Barents sea - paleoceanographic applications. Mar. Geol. 117, 303–316.
Stuiver, M., Braziunas, T.F., 1993. Modeling atmospheric ^{14}C influences and ^{14}C ages of marine samples to 10,000 BC. Radiocarbon 35, 137–189.
Stuiver, M., Reimer, P.J., 1993. Extended ^{14}C data-base and revised Calib 3.0 ^{14}C age calibration program. Radiocarbon 35, 215–230.
Svendsen, J.I., Alexanderson, H., Astakhov, V.I., Demidov, I., Dowdeswell, J.A., Funder, S., Gataullin, V., Henriksen, M., Hjort, C., Houmark-Nielsen, M., Hubberten, H.W., Ingolfsson, O., Jakobsson, M., Kjaer, K.H., Larsen, E., Lokrantz, H., Lunkka, J.P., Lysa, A., Mangerud, J., Matiouchkov, A., Murray, A., Moller, P., Niessen, F., Nikolskaya, O., Polyak, L., Saarnisto, M., Siegert, C., Siegert, M.J., Spielhagen, R.F., Stein, R., 2004. Late Quaternary ice sheet history of

northern Eurasia. Quat. Sci. Rev. 23, 1229–1271.
Thompson, W.G., Goldstein, S.L., 2006. A radiometric calibration of the SPECMAP timescale. Quat. Sci. Rev. 25, 3207–3215.
Vinje, T., 2001. Anomalies and trends of sea-ice extent and atmospheric circulation in the Nordic Seas during the period 1864-1998. J. Clim. 14, 255–267.
Vogt, C., 1997. Regional and temporal variations of mineral assemblages in Arctic Ocean sediments as climatic indicator during glacial/interglacial changes. Reports on Polar Research 251, 1–309.
Vogt, P.R., Crane, K., Sundvor, E., 1994. Deep pleistocene iceberg plowmarks on the Yermak plateau - sidescan and 3.5 Khz evidence for thick calving ice fronts and a possible marine ice-sheet in the Arctic-ocean. Geology 22, 403–406.
Vogt, C., Knies, J., Spielhagen, R.F., Stein, R., 2001. Detailed mineralogical evidence for two nearly identical glacial/deglacial cycles and Atlantic water advection to the Arctic Ocean during the last 90,000 years. Global Planet. Change 31, 23–44.
Volkman, J.K., 1986. A review of sterol markers for marine and terrigenous organic-matter. Org. Geochem. 9, 83–99.
Volkman, J.K., Barrett, S.M., Blackburn, S.I., Mansour, M.P., Sikes, E.L., Gelin, F., 1998. Microalgal biomarkers: a review of recent research developments. Org. Geochem. 29, 1163–1179.
Volkman, J.K., 2006. Lipid markers for marine organic matter. In: Volkman, K. (Ed.), Marine Organic Matter: Biomarkers, Isotopes and DNA. Springer, Berlin, pp. 27–70.
Volkman, J.K., Revill, A.T., Holdsworth, D.G., Fredericks, D., 2008. Organic matter sources in an enclosed coastal inlet assessed using lipid biomarkers and stable isotopes. Org. Geochem. 39 (6), 689–710.
Winkelmann, D., Schafer, C., Stein, R., Mackensen, A., 2008a. Terrigenous events and climate history of the Sophia Basin, Arctic Ocean. G-cubed 9, Q07023.
Winkelmann, D., Geissler, W., Schneider, J., Stein, R., Schenke, H.-W., 2008b. Dynamics and timing of the hinlopen/yermak megaslide north of Spitsbergen, Arctic Ocean. Mar. Geol. 250, 34–50.
Wollenburg, J.E., Kuhnt, W., Mackensen, A., 2001. Changes in Arctic Ocean paleoproductivity and hydrography during the last 145 kyr: the benthic foraminiferal record. Paleoceanography 16, 65–77.
Xiao, X.T., Fahl, K., Müller, J., Stein, R., 2015a. Sea-ice distribution in the modern Arctic Ocean: biomarker records from trans-Arctic Ocean surface sediments. Geochem. Cosmochim. Acta 155, 16–29.
Xiao, X.T., Stein, R., Fahl, K., 2015b. MIS 3 to MIS 1 temporal and LGM spatial variability in Arctic Ocean sea ice cover: reconstruction from biomarkers. Paleoceanography 30, 969–983.
Xuan, C., Channell, J.E.T., Polyak, L., Darby, D.A., 2012. Paleomagnetism of quaternary sediments from Lomonosov Ridge and Yermak plateau: implications for age models in the Arctic Ocean. Quat. Sci. Rev. 32, 48–63.